EUROPEAN ORGANIZATION FOR NUCLEAR RESEARCH

CERN-EP/88-98
9 August 1988

FIRST RESULTS OF ELECTRON COOLING EXPERIMENTS AT LEAR

H. Poth, W. Schwab, B. Seligmann, M. Wörtge and A. Wolf
Kernforschungszentrum Karlsruhe, Institut für Kernphysik,
Karlsruhe, Fed. Rep. Germany

S. Baird, M. Chanel, H. Haseroth, C.E. Hill, R. Ley,
D. Manglunki, G. Tranquille and J.L. Vallet
CERN, Geneva, Switzerland

P.F. Dittner
Oak Ridge National Laboratory, Oak Ridge, Tenn., USA

ABSTRACT

The first results are presented of electron cooling experiments in the Low-Energy Antiproton Ring (LEAR) at CERN, performed with a proton beam of about 50 and 21 MeV. The number of stored protons ranged from 10^7 to 3×10^9. Cooling times of the order of 1 s and proton drag rates of up to 0.7 MeV/s were obtained.

The capture of cooling electrons by protons producing hydrogen atoms was used to derive an effective electron temperature (0.25 eV). From the angular profile of the neutral hydrogen beam an upper limit of 3 π mm·mrad could be deduced for the horizontal equilibrium proton-beam emittance. The lowest equilibrium momentum spread was 2×10^{-5} (FWHM), as derived from the analysis of the longitudinal Schottky signal. This Schottky signal exhibited an unusual behaviour with beam intensity and under certain conditions showed a double-peak structure which was associated with collective beam noise.

For very cold beams transverse instabilities were observed, which resulted in a rapid spill-off of protons and a stabilization at lower intensities. The threshold of these instabilities was raised by heating the proton or the electron beam. The cooling of a bunched proton beam was investigated. The reduction of the proton momentum spread led to bunch lengths of about 2 m, containing 3×10^8 protons.

(Submitted to Zeitschrift für Physik A)

1. INTRODUCTION

In the last few years, electron cooling has gained considerable interest owing to its capability of rapidly increasing the phase-space density of stored ion beams by many orders of magnitude. This method was originally proposed by Budker [1], about twenty years ago. The first pioneering experiments were done at Novosibirsk in the mid-seventies [2], and then also in the ICE ring at CERN [3] and at Fermilab [4]. The great success of these first experiments, and the fast cooling rates obtained, motivated the application of electron cooling in the Low-Energy Antiproton Ring (LEAR) at CERN [5]. Later, the use of electron cooling was proposed for a number of other ion storage rings which are to come into operation in the late 1980s or the early 1990s.

The first generation of electron cooling experiments was done with protons, ranging in energy from 1.5 to 200 MeV and in intensity from 10^7 to 10^9 stored protons. A summary can be found elsewhere [6]. The aim of these experiments was to study the underlying dynamics and cooling forces. The results of the experiments were, in general, in agreement with the theory, developed mainly at Novosibirsk [7], at CERN [8], and at Aarhus [9]. Although electron cooling can be considered to be understood, there remain a number of open questions when cooling under extreme situations is investigated.

As one of the second generation of electron cooling experiments, the LEAR electron cooling project was faced with various technological problems such as, for instance, the development of a device for routine operation in a storage ring and the achievement of ultra-high vacuum conditions. The electron cooling device for LEAR was developed by a KfK-CERN Collaboration over the past few years; the stages of development were described on various occasions [10]. The cooling device produced its first electron beam at the beginning of 1985 and was studied in great detail before it was installed in LEAR. In this paper, we shall report on the results from the first cooling experiments performed with 50 MeV protons in October-November 1987, during 65 hours of beam time.

2. EXPERIMENTAL ARRANGEMENT

Protons accelerated to roughly 50 MeV ($\beta = 0.3$) in the Linac I at CERN were injected into the LEAR ring in a single turn. The electron cooler is situated in straight section 3 (SL3) (Fig. 1). The electron beam, generated in an electron gun and accelerated to about 27 keV in order to match the proton velocity, is transported in a solenoid field and inflected into the proton beam by a toroidal section of the electron cooler magnet. After 1.5 m it is separated from the protons in another toroid magnet and transported to a collector. A detailed description of the electron cooling device developed for LEAR can be found in Ref. [10]. Typical operation parameters for the electron cooler are given in Table 1.

On each side of the cooler a horizontal and a vertical dipole in LEAR permitted the correction of the deflection in the toroids and steering of the proton beam in the electron cooling device. Electrostatic pick-up stations, distributed all around the ring, offered the possibility of measuring the position of the protons when bunched. At the positions indicated in Fig. 1, Schottky pick-up electrodes are installed. The Schottky signal is the noise induced by the beam particles in the electrode that represents the density fluctuation in a coasting beam. In usual Schottky spectra, the width of the signal is proportional to the momentum spread in the beam, and the signal amplitude is proportional to the square root of the beam intensity (Schottky signals will be discussed later in more detail). Upstream of the cooler a beam-current transformer measures the beam intensity. In order to observe the neutral hydrogen beam, created in the cooling section when cooling electrons are captured by circulating protons, a detection system is mounted at the extension of the vacuum tube of SL3. It consists of a multiwire proportional chamber (MWPC) with two planes and a stack of three scintillators. The MWPC covers an area of 10 cm x 10 cm and has a wire spacing of 6 mm. The sizes of the scintillators are 10 cm x 10 cm and their thicknesses in the beam direction are 5 mm, 1 cm, and 1 cm, respectively. Two radio-

frequency (RF) cavities, situated in SL4, are used to bunch and to decelerate the proton beam. The LEAR machine parameters [11] relevant to this experiment are summarized in Table 2.

3. ELECTRONIC EQUIPMENT AND CONTROLS

The Schottky signals were analysed with fast spectrum analysers (HP8568A) as used in the standard operation of LEAR. The MWPCs for the neutral-beam profile measurements are read out every second in analog mode after a correspondingly long integration time. The signals from the scintillators are passed through discriminators and are timed for coincidence. The singles and the coincidence rates were measured with NIM scalers and a rate meter. A timing signal, derived from the RF, was used to stop a time-to-digital converter (TDC), which was started by the coincidence. The output of the TDC was fed into a multichannel analyser (MCA) giving the time distribution of the neutrals for a bunched proton beam.

The proton orbit was determined with the above-mentioned pick-ups, and the corresponding electronics as used in general for LEAR. The position of the electron beam was obtained from pick-ups installed in the cooler. In order to receive a signal the acceleration voltage, and by that the electron current, was modulated. Also the proton-beam position could be determined via these pick-ups.

The acceleration voltage was measured via a precise resistive divider, which was connected to a 16-bit ADC as well as a differential voltmeter. The latter enabled us to observe high-voltage variations as low as 0.1 V at frequencies lower than 1 Hz.

The LEAR machine was controlled through its normal operating system from the LEAR control room. The electron cooler had its own operation system, based on an LSI 11/23 and on CAMAC and NIM electronics. It was operated via a dedicated terminal from the LEAR control room, where all important parameters of the electron cooler were displayed on a video screen.

4. ELECTRON COOLING EXPERIMENTS

4.1 The proton beam prior to cooling

The magnetic field in the toroids of the cooler, bent in the vertical plane, presents a horizontal force component to the proton beam which deflects it to the same side at the entrance and the exit of the cooler. This horizontal deflection is

$$\theta_x = \int (B_z ds/B\varrho) , \qquad (1)$$

with $B\varrho$ being the proton-beam rigidity, B_z the vertical magnetic field component, and s the path length of the protons in the toroid. The integral was previously determined in a magnetic-field measurement [12] and found to be B_0 x 0.234 m for each toroid. (B_0 is the longitudinal field in the solenoid). This deflection amounts to 10 mrad, and is independent of the particle momentum since the magnetic field of the cooler is scaled proportionally. The effect was compensated by retuning the dipole magnets DEH31, DEH32, DWH22, and DWH21 (Fig. 1). The proton-beam position was measured in the cooling section with the pick-ups, and found to be parallel to the vacuum chamber but displaced from its centre by 6 mm. The change of the betatron tune after the orbit adjustment was less than 10^{-3}.

The magnetic field of the solenoid of the cooler causes a small azimuthal rotation of the proton beam. The rotation angle θ_a per passage is given by the integral over the longitudinal field B_s in the solenoid and the toroids,

$$\theta_a = \int B_s ds/2B\varrho , \qquad (2)$$

and amounts to 65 mrad. This results in the excitation of a betatron resonance at $Q_h + Q_v = 5$, which is close to the working point. The width of this resonance is $\Delta Q = 7 \times 10^{-3}$. The difference in tune in the horizontal and the vertical betatron phase space causes a beating of the betatron oscillations. The effect can be observed by measuring the signal of a bunched beam on an electrostatic pick-up after a

kick. Figure 2 shows this beating for a solenoid field of 455 G without electron beam.

4.2 Relevant electron-beam properties

The electrons are accelerated in an electron gun. Shielding of the inner electrons leads to a depression of the acceleration voltage across the electron beam, which results in a radial variation of the longitudinal velocity. The energy of an electron at a given radial position is

$$E(r) = E_0 + n_e \pi r^2 r_e mc^2 , \qquad (3)$$

where E_0 is the electron energy on the beam axis:

$$E_0 = eU - n_e \pi a^2 r_e mc^2 [1 + 2 \ln(b/a)] . \qquad (4)$$

Here U is the potential difference between the cathode and the vacuum tube surrounding the beam, e the elementary charge, b (= 7 cm) the radius of the vacuum tube, a the electron-beam radius, r_e the classical electron radius, m the electron mass, n_e the electron density, and c the velocity of light. The situation is illustrated in Fig. 3 by the parabola. The negative charges might be compensated by trapping positive ions in the electron beam. In this case one has to replace n_e by $(1 - x)n_e$, where x assumes a value between zero and unity describing the degree of space-charge compensation.

The electron beam was parallel to the vacuum chamber and centred within 0.5 mm as verified with the pick-ups. In the following the cooling experiments will be described in detail.

4.3 Cooling of coasting proton beams at 308.6 MeV/c

4.3.1 Cooling of a newly injected beam

Figure 4a shows the frequency spectrum of the coasting proton beam derived from the longitudinal Schottky pick-up just after injection into LEAR. The spectrum shows the region around the 35th

harmonic of the revolution frequency. The width Δf of the spectrum is related to the width of the momentum distribution by

$$\Delta f/f = \eta \, \Delta p/p \ . \tag{5}$$

The FWHM momentum spread $\Delta p/p$ can be related to a longitudinal proton-beam temperature (in eV) by

$$T_{p,\parallel} = \frac{1}{4 l n^4} \, Mc^2 \, \beta^2 (\Delta p/p)^2 \ , \tag{6}$$

where M is the proton mass.

The initial momentum spread was about 3×10^{-3}, which is equivalent to about 800 eV. The protons are distributed along the straight line shown in Fig. 3. This straight line represents the momentum dispersion in the cooling section. The momentum dispersion D connects the momentum deviation δp of a proton of the nominal beam momentum p with the radial position r in the electron beam by

$$r = D \, \delta p/p \ . \tag{7}$$

(To simplify the argument, the vertical displacement of the protons from the electron-beam axis is neglected, and this axis is assumed to coincide with the nominal proton orbit).

Electron cooling reduces the velocity difference between the particles of both beams. Hence the protons are dragged to the crossing point between the straight line and the parabola. The radial position of the crossing point depends on the electron acceleration voltage and the space-charge fields.

In order to achieve cooling, the electron velocity has to be adjusted to a crossing point within the machine acceptance. In a previous experiment, where the radial velocity distribution of the electron beam was investigated, we found a negligible space-charge compensation [13]. Therefore, the acceleration voltage U was set such that the central electrons had an energy (E_0) of 26.929 keV, resulting in a velocity equal to that of protons on the nominal orbit.

Before injection the electron-beam energy was set about 2 keV lower than E_0. Then, at a given moment after injection, the electron energy was stepped up to E_0 and the proton beam was cooled. Within a few seconds the equilibrium distribution, as shown in the second trace of Fig. 4a, was reached. The position of the narrow peak corresponds to a situation with vanishing space-charge compensation in the electron beam ($x = 0$). The time evolution can be seen for another injection and cooling cycle in Fig. 4b showing frequency scans every second.

4.3.2 Neutral hydrogen formation rate

In electron cooling of protons, electrons are occasionally captured by the protons and hydrogen atoms are formed. These neutral systems leave the ring in the extension of the cooling straight section (SL3) and are detected outside the magnets. The hydrogen-formation rate R_H is related to the effective temperature of the electrons by [14]

$$R_H = N_p(\ell/C)\alpha_r n_e \gamma^{-2} \quad , \tag{8}$$

with the recombination coefficient α_r given by

$$\alpha_r = 9.2 \times 10^{-14} \text{ cm}^3 \text{ s}^{-1} \sqrt{(13.6 \text{ eV}/T_e)}$$

$$\times \left[0.43 + 0.48(T_e/13.6 \text{ eV})^{1/3} + 0.5 \ln (13.6 \text{ eV}/T_e)\right] . \tag{9a}$$

Here T_e is the temperature associated with the relative motion between electrons and protons. The dependence of the recombination coefficient on T_e can be simplified for our purpose to [14]

$$\alpha_r = 0.8 \times 10^{-12} \text{ cm}^3 \text{ s}^{-1} T_e^{-0.645} . \qquad (T_e \text{ in eV}) \tag{9b}$$

One can define a normalized count rate α_0 by dividing the neutral hydrogen rate by the electron current $I_e = n_e \pi a^2 e \beta c$ (in A) and by the proton-beam current $I_p = (N_p/C) e \beta c$ (in mA):

$$\alpha_0 = R_H/(I_e I_p) = 3125 \text{ s}^{-1} \alpha_r \qquad (\alpha_r \text{ in } 10^{-12} \text{ cm}^3 \text{ s}^{-1}) \tag{10a}$$

or

$$\alpha_0 = 2500\ s^{-1}\ T_e^{-0.645} \qquad (T_e \text{ in eV}) \ . \tag{10b}$$

We measured α_0 and obtained an average value of $\alpha_0 = (6100 \pm 600)\ s^{-1}$. Since for perfectly aligned beams and a low momentum spread of the proton beam, T_e corresponds to the electron temperature, we can give an upper limit for the transverse temperature:

$$T_e = (2500\ s^{-1}/\alpha_0)^{1.55} = 0.25(4)\ \text{eV} \ . \tag{11}$$

4.3.3 Equilibrium proton-beam divergence

The neutral hydrogen beam was also used to measure the angular profile of the cooled proton beam. The vertical and horizontal distributions measured with the MWPC are shown in Fig. 5. The standard deviations $x_{h,v}$ of the distributions are related to the proton-beam divergence $\theta_{h,v}$ in the following way:

$$\theta_{h,v} = x_{h,v}/\sqrt{(L^2 + \beta_{h,v}^2)} \ . \tag{12}$$

Because the resolution of the chamber was 6 mm, only an upper limit for $x_h < 8$ mm and $x_v < 9$ mm can be given. From the LEAR parameters of Table 2 and Eq. (12) we have

$$\theta_h < 0.84\ \text{mrad} \quad \text{and} \quad \theta_v < 0.84\ \text{mrad}. \tag{13}$$

From these divergences we can calculate the transverse proton-beam temperature

$$T_{p,\perp} = \frac{1}{2} Mc^2\ \beta^2\gamma^2\ (\theta_h^2 + \theta_v^2) < 70\ \text{eV} \ . \tag{14}$$

A comparison with Eq. (11) shows that thermal equilibrium is probably not reached. Note, however, that Eq. (14) represents only an upper limit and the temperature depends quadratically on the divergence.

The emittance (containing 63% of all particles) is related to the divergence by

$$\varepsilon_{h,v} = 2\theta^2 \beta_{h,v} \cdot \qquad (15)$$

We therefore get an upper limit for the emittances (63%):

$$\varepsilon_h < 2.7\pi \text{ mm·mrad}, \quad \varepsilon_v < 7.5\pi \text{ mm·mrad} \qquad (16)$$

and for the proton-beam radius in the cooling section ($a_{h,v} = \beta_{h,v}\theta$):

$$a_h < 1.6 \text{ mm} , \quad a_v < 4.5 \text{ mm} . \qquad (17)$$

These values were obtained for 1×10^9 circulating protons.

4.3.4 Measurement of the longitudinal frictional force

The longitudinal frictional force was measured in different ways. For small differences in velocity between protons and electrons the following procedure was applied. The acceleration voltage of the electron beam was suddenly stepped up by ΔU. Consequently, the protons were accelerated and their revolution frequency increased. At the same time as the voltage was stepped up the spectrum analyser was triggered. A narrow frequency band was selected and the intensity in this band was monitored as a function of time. When the revolution frequency passed this band a signal, as shown in Fig. 6a, was observed if the position of the frequency band was in between the initial and the final frequency. In the case where it was set to the final frequency, the signal shown in Fig. 6b was seen. From these measurements the rate of frequency change, and from that the frictional force, was determined. The measurements are summarized in Fig. 7. The length of the cooling region relative to the ring circumference has been taken into account by multiplying the observed proton drag rates by C/ℓ. The highest drag rate, observed at the lowest relative velocity, was 0.7 MeV/s.

It should be noted that the measurement of the frictional force for small velocity differences is very difficult because of the rapid changes of the particle velocities. The precision obtained in the voltage-step measurement is limited by the fact that the frictional force changes with decreasing velocity difference after the step. For

the plot we always took the velocity difference corresponding to the full step.

4.3.5 Longitudinal cooling time

In contrast to what was described before, we also measured the time it took to cool to equilibrium a longitudinally blown-up beam. After cooling of the proton beam, the electron acceleration voltage was stepped down by 2 kV in order to deactivate cooling. Next the proton-beam momentum spread was increased by feeding noise on to a Schottky kicker (stochastic heating). This noise extended over a narrow band around a harmonic of the revolution frequency. The protons randomly change their momentum within this band, where the speed of the diffusion is determined by the noise amplitude. After some seconds, a rectangular distribution as shown in Fig. 8 was reached. The stochastic heating was stopped and the shape of the momentum distribution remained. Thereafter the acceleration voltage of the gun was put back to the matched value and the spectrum analyser was triggered at the same time. The latter measured the intensity within a certain band around the final frequency as a function of time. This dependence is displayed in Fig. 9. The measurement was repeated for different initial momentum spreads and we extracted the time it took until a constant level of the noise intensity was reached (Fig. 10). We assumed that the increase of the Schottky signal in Fig. 9 stops when the majority of particles has been cooled to the final momentum (shown by the second trace in Fig. 8). In this case, the values shown in Fig. 10 are the total cooling times. These results are very small compared with the cooling of a newly injected beam. Shorter cooling times are, of course, expected (since the beam is already cold in the transverse direction) but not by more than one order of magnitude. It should be noted that, with this method, we cannot exclude that particles contained in the tails of the distribution might be neglected. Yet fast frequency scans immediately after the onset of the cooling action gave no

indication of that. Since the cooling time becomes constant when the proton-electron velocity spread is dominated by the electron velocity spread, we could also derive an upper limit of the longitudinal electron temperature, which is 0.014 eV.

The constant noise level, reached after a very short time, could also be caused by the collective suppression of beam noise as discussed in Section 4.3.11 and described, in particular, by Eq. (23).

4.3.6 Counteracting of the proton-beam heating with electron cooling

In this measurement the stochastic heating was left on while the electron cooling was reactivated by putting the acceleration voltage back to the matched value. Since the cooling had now to fight against a major heating source, it took much longer to reach equilibrium and the final momentum spread was larger than without heating. The different equilibrium values between stochastic heating and electron cooling are shown in Fig. 11 for various heating levels. The longitudinal velocity distribution of the protons resulting from simultaneous cooling and heating can be described by a Fokker-Planck equation, independent of the proton velocity within the noise band, and a frictional term depending on the velocity of the protons relative to that of the electrons. This friction term represents the cooling force. Using the measured shape of the proton velocity, it should be possible, from this measurement, to determine the frictional force as a function of the relative velocity. This method also provides a precise reference measurement for later experiments with antiprotons.

4.3.7 Heating of the electron beam

In order to study the cooling dependence on the electron temperature, the electron beam was heated in the longitudinal direction by modulating the acceleration voltage. The modulation frequency was fixed at the maximum transmission of the electric circuitry of the

high-voltage power supply (4 kHz). The heating of the electron beam led to different equilibrium momentum spreads in the proton beam. They are plotted in Fig. 12 as a function of modulation amplitude for the acceleration voltage of the electrons. The modulation amplitude can be translated into a 'longitudinal electron temperature' by

$$\tilde{T}_{e,\parallel} = \frac{2T_C^2 + E^2(\Delta U/U)^2}{8E(\gamma + 1)} \approx \frac{E}{16}\left(\frac{\Delta U}{U}\right)^2 , \qquad (18)$$

where the last expression holds when the cathode temperature T_C can be neglected [$T_C << E(\Delta U/U)$].

This temperature is not to be identified with the electron temperature in a thermodynamical sense relevant to cooling. Hence we investigated the dependence of the equilibrium proton temperature on the modulation amplitude. The modulation amplitude ΔU (peak-to-peak) ranged from 160 V to 10 kV, corresponding to a range of $\tilde{T}_{e,\parallel}$ from 0.06 eV to 230 eV. On the other hand, the momentum spread of the protons is related to their longitudinal temperature by Eq. (6). If one assumes that thermal equilibrium is reached, one would expect the proton momentum spread to be given by

$$\frac{\Delta p}{p} = \frac{\Delta U}{U}\frac{1}{4\beta}\sqrt{\frac{E \ln 4}{Mc^2}} \approx 5 \times 10^{-3}\,\frac{\Delta U}{U} \qquad (19)$$

for $E(\Delta U/U) >> T_C$. This straight line can be found in Fig. 12.

The longitudinal heating of the electron beam should also lead to a decrease in electron-proton recombination [Eqs. (8) and (9)]. This dependence was measured and is shown in Fig. 13.

When the longitudinal proton temperature is increased by modulating the electron energy, also the transverse emittance should increase because one expects intrabeam scattering to equalize the temperatures. Another possibility for transverse heating could be the cooling process itself in the case where the transverse temperature is much lower than the longitudinal one and the transverse magnetic cooling force changes sign. We did not study this quantitatively but observed an increase of emittance when the electron beam was modulated with a large amplitude.

4.3.8 Variation of electron current

The cooling force should depend linearly on the density (current) of the electrons if their temperature remains unchanged. We briefly checked this by reducing the electron current to about one half and one quarter of its nominal value. This was achieved by reducing the heating of the cathode correspondingly. The procedure should lead to a slight beam heating since transverse electric field components appear close to the cathode in the case of temperature-limited emission. We measured the hydrogen-formation rate, which as stated in Eq. (8) depends on the electron temperature for various beam currents, and did not observe significant electron-beam heating.

Since the opening of the velocity parabola changes with the electron current, as seen from Eqs. (3) and (4), the crossing point seen in Fig. 3 should move differently with the electron acceleration voltage for the three currents. The measured revolution frequency of the cooled beam as a function the electron acceleration voltage, shown in Fig. 14, exhibits deviations from the value given by the position of the crossing point, which may indicate that both beams are not yet fully aligned. The acceleration voltage U_0, for which the electron beam energy on axis (E_0) corresponds to the nominal revolution frequency f_0, is indicated by arrows and shifts with the electron-beam current [see Eq. (4)]. The measured shifts indicate no space-charge compensation.

4.3.9 Transverse cooling

Only the relative change in the transverse phase space could be observed by watching the side-bands of the Schottky signal induced in transverse pick-up electrodes. A beam with finite emittance produces side-bands on each side of a central peak, corresponding to the revolution frequency (Fig. 15a). The frequency difference between two consecutive satellites is related to the fractional value of the betatron tune. The height of the satellite peaks of the transverse Schottky signal relative to the height of a peak of the longitudinal

Schottky signal is proportional to the square root of the beam emittance, taking into account the noise level. Owing to transverse beam cooling these satellites disappear when the beam becomes cold in the transverse direction (Fig. 15b).

We measured the intensity decrease of these peaks as a function of time (Fig. 16) and determined the approximate transverse emittance cooling time; it was found to be about 1.5 s.

4.3.10 Instabilities

As described above, the cooling of a newly injected beam led, within a few seconds, to an increase in phase-space density by more than four orders of magnitude. During this period only small losses occurred. However, when the proton beam reached a certain temperature and the initial intensity was high (the injected intensity varied by a factor of five), we occasionally observed instabilities which removed a fraction of the beam particles. The beam intensity thereafter remained constant and the instabilities did not reappear. In the transverse Schottky signal a precursor of this situation was often seen: first the side-bands decreased normally and disappeared as an effect of transverse cooling, then suddenly satellites appeared at different positions on either side of the central peak (Fig. 15c). In many cases the losses occurred soon after that.

The intensity of the beam stabilized at a value of about 7×10^8 after the beam losses. We tried to avoid the losses by continuous (longitudinal) stochastic heating of the proton beam. Although the heating acted only on the momentum spread, the emittances might have been increased through intrabeam scattering. It was found that the instability threshold could be raised by increasing the heating of the proton beam. In this way, stable conditions were found for stored beam intensities of up to 2.2×10^9 protons. A similar result was obtained by modulating the acceleration voltage of the electron beam.

4.3.11 Investigation of the longitudinal Schottky signal

The longitudinal cooling of the proton beam to low temperature led to the observation of an unusual noise spectrum of the coasting beam observed by the longitudinal pick-up. For a cold beam the signal was no longer Gaussian but deformed into the double-peak structure as shown in Fig. 17a. It could be excluded that this structure might be caused by a misalignment of the two beams. The splitting of the signal and the depth of the dip varied with the beam intensity. The intensity of the Schottky signal barely depended on the beam intensity.

A similar observation was reported from cooling experiments at Novosibirsk [15]. An explanation of the signal behaviour, given elsewhere [16], can be summarized roughly as follows. The beam-noise signal represents the density fluctuation in a coasting beam. For the shot noise of independent beam particles, the spectral width of the signal is proportional to the momentum spread in the beam and the signal strength is proportional to the square root of the spectral power density. When the beam temperature decreases to very low values, as achieved with electron cooling, the beam particles can no longer be considered as being independent, and density fluctuations decrease rapidly. The energy of the particles in the rest frame becomes comparable to the electric force they exert upon each other, and their mutual repulsion hinders the development of density fluctuations. Therefore the signal should decrease with decreasing temperature for constant beam intensity.

In particular, the relevant electromagnetic interaction between the beam particles is expressed by the frequency-dependent longitudinal coupling impedance $Z(f)$ of the machine [17]. The time evolution of the collective motion which dominates the density fluctuations at a low proton temperature is described by a characteristic frequency f_c depending on the number of stored protons N_p and on Z. These collective fluctuations can be considered as two waves moving with or against the direction of the beam. The appearance of these waves

removes strength from the centre of the Schottky signal to its tails, resulting in the shape shown in Fig. 17. Accordingly, the spectral density of the noise signal observed near the n-th harmonic of the nominal revolution frequency f_0 is concentrated in two peaks at $n\bar{f} \pm f_c$, where $\bar{f} \approx f_0$ is the mean revolution frequency of the protons. The characteristic frequency f_c is given by

$$\frac{f_c}{nf_0} = e\sqrt{\frac{\eta N_p}{pC}}\,\frac{iZ_n}{n} \quad . \tag{20}$$

The main contribution to the coupling impedance $Z_n = Z(nf_0)$ in the relevant frequency range is the space-charge impedance of a beam of radius a in a circular vacuum chamber of radius b:

$$Z_n = i\,n\,Z_0\,\frac{1 + 2\,\ln(b/a)}{2\beta\gamma^2} \quad , \tag{21}$$

Z_0 being the impedance of the vacuum (377 Ω).

If f_c is small compared to the spread of the revolution frequency, Δf, the usual Schottky spectrum is observed. A *collective* noise spectrum with a reduced total intensity occurs if $f_c > n\Delta f$. For the critical particle number at which $f_c = n\Delta f$ one obtains

$$N_{cr} = \frac{\eta}{iZ_n/n}\,\frac{C\,\Delta p^2}{e^2 p} \quad . \tag{22}$$

The total noise amplitude $\langle A^2 \rangle$ behaves as [16]

$$\langle A^2 \rangle = \begin{cases} N & \text{for } N \ll N_{cr} \\ N_{cr} & \text{for } N \gg N_{cr} \end{cases} \quad . \tag{23}$$

Hence, in the range of low longitudinal proton temperature, the integrated noise power becomes independent of the proton current and depends only on the proton temperature.

The procedure used to determine the frequency spread Δf, and hence the momentum spread, of the coasting beam is described in the Appendix. The calculated spectra of the noise voltage are shown in Fig. 17b with the momentum spread as a parameter. The distance between the maxima, and the relative depth of the dip are displayed

in Figs. 17c and d as a function of the ratio $\Delta f/f_c$. As explained in the Appendix, these curves are used in order to derive the momentum spread from the experimental spectra. The results are plotted as a function of beam intensity in Fig. 18. The impedance Z_n/n was determined from these measurements to be about 500 Ω.

Also in Fig. 18 are shown the data obtained in the ICE ring and at Novosibirsk (NAP-M). The equilibrium momentum spreads obtained now are lower than those measured in ICE.

4.4 Cooling of the bunched proton beam

The cooling of a bunched proton beam was studied under various conditions. The emphasis was again put on the investigation of the longitudinal phase space. Care was taken to synchronize the RF with the electron energy. This was achieved by adjusting the high voltage of the electron gun such that the coasting proton beam was cooled to a revolution frequency corresponding to the RF. Then the RF was turned on and the bunch signal from a position pick-up station was observed, which showed a narrow spike corresponding to a short bunch. The following measurements were aimed at the determination of the longitudinal cooling time, the equilibrium emittances for a bunched beam, and the bunch length as a function of the RF amplitude.

4.4.1 Longitudinal cooling time

The beam was injected and adiabatically bunched with the electron cooling inactive (high voltage 2 kV lower than required for cooling). Then the electron velocity was matched by stepping up the high voltage, and the shrinkage of the pulses, induced by the bunches on a position pick-up, was observed. The decrease of the momentum spread, caused by the cooling, reduced the bunch length and increased the signal amplitude. The change of the signal amplitude with time was observed at a higher harmonic of the revolution frequency (Fig. 19) and used to deduce the total longitudinal cooling time for a bunched beam. For these measurements the beam intensity was

typically about 4 x 10^8 and stable. The total longitudinal cooling time obtained was 3 s.

4.4.2 Bunch length

The decrease in the momentum spread of the bunched beam through longitudinal cooling resulted in a reduction of the bunch length, as witnessed by Fig. 19. The relation between bunch length ℓ_b, momentum spread, and RF voltage amplitude is as follows:

$$U_{RF} = (\pi/2)\eta\beta^2\gamma(\Delta p/p)^2 \ (0.625 \ C/\ell_b)^2 \ \frac{Mc^2}{e} \ x \ 10^{-6} \ . \qquad (24)$$

Note that the bunch area A of the circulating beam

$$A = \pi^2\beta\gamma\ell_b \frac{\Delta p}{p} \frac{\ell}{C} \ , \qquad (25)$$

cannot be considered to be constant in the presence of cooling when passing from coasting to bunched beam. Therefore $\Delta p/p$ and ℓ_b have to be treated as independent parameters.

The hydrogen beam formed by electron capture is pulsed in the case of a bunched beam. We profited from that and determined l_b from the distribution of the arrival times of the H_0 atoms (the electron was stripped off in the window at the end of the vacuum chamber) in the scintillator telescope. The scintillator signal started a TDC, which was stopped by a signal derived from the RF. The time spectrum of the atoms shows (Fig. 20) a clean Gaussian peak and little background, indicating that all protons are captured in the stationary bucket. The bunch length measured as a function of the RF voltage is shown in Fig. 21.

The average hydrogen-formation rate and the beam profile were also determined in the case of a bunched beam. The hydrogen rate remains nearly constant, indicating that the beam is hardly heated by increasing U_{RF}. The measured recombination rate corresponds to a transverse temperature of 0.32 eV. Furthermore, the beam size appeared to be the same as for a coasting beam. The compression of the coasting beam into a stable bunch of about 2.5 m, containing

about 4 x 10^8 protons, corresponds to 1.3 x 10^{10} protons in a coasting beam.

4.5 Cooling at 200 MeV/c

The cooling of protons stored at 200 MeV/c was only briefly studied since it involved a great deal of machine gymnastics. The proton beam was injected at 300 MeV/c with the electron cooling device turned off (including the magnetic field). The beam was RF captured and the normal LEAR deceleration cycle was used to bring the proton beam to the 200 MeV/c flat top. Then the electron-beam energy was increased in small steps and the correction dipoles were adjusted correspondingly at each step. After about five steps the 11 kV of the electron beam was reached and cooling was observed. A proton beam with an initial $\Delta p/p$ of 2 x 10^{-3} was cooled in momentum space within 4 s to less than 2 x 10^{-4}.

5. SUMMARY AND CONCLUSION

The electron cooling of protons circulating in LEAR was studied in some detail. Most measurements were done at a momentum of 300 MeV/c and proton intensities of around 10^9. Depending on the initial conditions, cooling times of between 75 ms and 3 s were obtained. The equilibrium beam radii in the cooling section were less than 1.6 mm (horizontal) and 4.5 mm (vertical); the divergence was smaller than 0.8 mrad. Collective longitudinal noise spectra of unusual shape were observed and analysed. The lowest momentum spread obtained from them was 2 x 10^{-5} (FWHM). Typical rates for hydrogen-atom production through electron capture of protons were of the order of a few thousand per second. The short cooling times and small equilibrium emittances measured are in accordance with previous estimates and confirm the high quality of the electron beam. It was shown that electron cooling can increase the phase-space density of particle beams stored in LEAR by many orders of magnitude within a few seconds. The reduction of the proton-beam emittances to low

values, for high beam intensities, led to transverse instabilities. They were studied in a later run in more detail. Also bunched beams were cooled and similar cooling times and equilibrium emittances as for coasting beams were obtained. The compression of the coasting beam into a bunch of 2 m length corresponded to a cooling of 1.5×10^{10} protons in a coasting beam.

The electron cooling for LEAR was developed in order to allow the operation of an internal target at low energy and to facilitate the deceleration of antiprotons to very low energy. Also the short bunches obtained with the help of electron cooling are of interest for experiments which aim at trapping antiprotons at thermal energies. The fast cooling times and low beam equilibrium properties confirm that the goals set for electron cooling have been met.

APPENDIX

Evaluation of longitudinal Schottky noise spectra of dense, cold beams

The Schottky noise spectrum in a stored proton beam at the harmonic number n, as a function of the observed frequency f, is described by the Fourier transform of the longitudinal charge density $\varrho_n(f)$. When the interaction of the protons is neglected, let the charge density be given by the stochastic fluctuation (shot noise) spectrum $\varrho_{0,n}(f)$. The modification of the charge-density fluctuation by the electromagnetic interaction between the protons can then be described by introducing the dielectric function $\varepsilon_n(f)$ which, by definition, relates the disturbed and undisturbed spectra in the following way:

$$\varrho_n(f) = \varrho_{0,n}(f)/\varepsilon_n(f) \ . \qquad (A.1)$$

Expressing the particle interaction by the longitudinal coupling impedance Z_n, using the linearized Boltzmann equation, and relating the revolution frequency f_r to the momentum p of the protons by $df_r/dp = \eta f_0/p$, one obtains [16]

$$\varepsilon_n(f) = 1 - \left[\frac{(iZ_n/n)\eta(N_p/C)e^2 f_0^2}{p}\right] \int \frac{[\partial F(f_r)/\partial f_r]df_r}{(f/n - f_r)} \ , \qquad (A.2)$$

where $F(f_r)$ is the normalized distribution of the revolution frequencies of the beam.

The special case of a Gaussian distribution $F(f_r)$ of width Δf around the nominal revolution frequency f_0 will now be considered. In this case, Eq. (A.2) reduces to

$$\varepsilon_n(t) = 1 + (s^2/\sqrt{\pi}) \int u\, e^{-u^2}\, du/(u-t) \ , \qquad (A.3)$$

where $t = (f - nf_0)/(\sqrt{2}\, n\Delta f)$, $s^2 = f_c^2/(n\Delta f)^2$, and $f_{c,n}$ is the coherent frequency defined by Eq. (20). The discussion will be limited to

a situation where f_c is real; this implies that $\eta > 0$ and that Z_n is purely capacitive as given by the space-charge impedance alone.

For the evaluation of the experimental noise spectra, the general result of Eq. (A.3) is used instead of the limits for $s \ll 1$ or $s \gg 1$ given in previous papers [16, 18]. This general result can be written as

$$\varepsilon_n(t) = 1 + s^2[1 - 2tD(t) + i\sqrt{\pi}t\, e^{-t^2}] , \qquad (A.4)$$

where $D(t) = e^{-t^2} \int_0^t e^{u^2} du$ is a tabulated function [19], often called Dawson's integral. The spectrum of the voltage observed on a pick-up electrode sensitive to longitudinal charge-density fluctuations is finally described by

$$U_n(t) \propto |\varrho_n(t)| \propto e^{-t^2/2}/|\varepsilon_n(t)| , \qquad (A.5)$$

where the fact has been used that, for the shot-noise spectrum, $|\varrho_{0,n}(f)|^2 \propto F(f_r)$.

The theoretical spectral shape, shown in Fig. 17b, has prominent geometrical properties which can be compared with experimental spectra for their evaluation. Therefore, the peak spacing d and the ratio of the amplitude at the central minimum to the maximal amplitude, $r = U_n(0)/U_n(d/2)$, have been determined numerically as functions of the parameter s (see Figs. 17c and d). Since the function r(s) is monotonous, an experimental value of s, called s_{exp}, can be found from the measured value of r. Using the theoretical function d(s), the revolution frequency spread Δf can then be determined by dividing the measured frequency splitting of the noise spectrum by $\sqrt{2}\, n\, d(s_{exp})$. This yields the relative momentum spread (FWHM) given by $2\, \eta\, \Delta f/f_0$.

In this analysis, the measured amplitude ratio corresponds to the theoretical value r only if the resolution bandwidth of the spectrum analyser is sufficiently small to resolve the spectral shape. This can be verified by comparing the observed widths of the

doublet peaks with the spectral resolution. Only signals where the peak width exceeded the resolution bandwidth were used in the analysis.

Besides the momentum spread of the proton beam, this evaluation of the noise spectra also yields the longitudinal coupling impedance if the stored proton current and η are known from independent measurements. For a series of measurements under similar conditions, the observation of a constant value of Z_n provided a useful consistency check.

REFERENCES

[1] G.I. Budker, Proc. Int. Symposium on Electron and Positron Storage Rings, Saclay, 1966 (Presses Universitaires de France, Paris, 1967), p. II-1-1.

[2] G.I. Budker et al., Part. Accel. 7 (1976) 197.

Ya. Derbenev and I. Meshkov, CERN 77-08 (1977).

N.S. Dikansky et al., The study of fast electron cooling, INP preprint 79-56 (1979).

V.V. Parkhomchuk et al., Measurement of momentum cooling rates with electron cooling at NAP-M, INP preprint 78-81 (1978).

[3] M. Bell et al., Phys. Lett. 87B (1979) 275.

M. Bell et al., Nucl. Instrum. Methods 190 (1981) 237.

[4] R. Forster et al., IEEE Trans. Nucl. Sci. NS-28 (1981) 2386.

T. Ellison et al., IEEE Trans. Nucl. Sci. NS-30 (1983) 2636.

[5] H. Haseroth, Ch. Hill, P. Møller-Petersen and H. Poth, On the use of the ICE gun in LEAR, CERN PS/LR/Note 80-7 (1980).

W. Hardt et al., Design study of a facility for experiments with low energy antiprotons (LEAR), CERN/PS/DL 80-7 (1980).

[6] A.N. Skrinsky and V.V. Parkhomchuk, Sov. J. Part. Nucl. Phys. 12 (1981) 223.

F.T. Cole and F.E. Mills, Ann. Rev. Nucl. Sci. 31 (1981) 295.

H. Poth, Review of cooling experiments, in Proc. Workshop on Electron Cooling and Related Applications (ECOOL84), Karlsruhe, 1984, KfK 3846 (1984).

[7] Ya. Derbenev and A.N. Skrinsky, Part. Accel. 8 (1977) 1 and 235.

[8] M. Bell, Part. Accel. 10 (1980) 101.

J.S. Bell and M. Bell, Part. Accel. 11 (1981) 233.

[9] A.H. Sørensen and E. Bonderup, Nucl. Instrum. Methods 215 (1983) 27.

[10] C. Habfast, H. Haseroth, C.E. Hill, H. Poth, W. Schwab, B. Seligmann, M. Wörtge and A. Wolf, The LEAR electron cooler: recent improvements and tests, Phys. Scr. T22 (1988) 277.

H. Poth, C. Habfast, W. Schwab, B. Seligmann, M. Wörtge, A. Wolf, H. Haseroth, C.E. Hill and J.L. Vallet, The electron cooling device developed for LEAR, Proc. 4th Workshop on Physics at LEAR with Cooled Low Energy Antiprotons, Villars sur Ollon, 1987 (Harwood Academic, Chur, 1988), p. 121.

[11] P. Lefèvre et al., LEAR, Proc. 4th Workshop on Physics at LEAR with Cooled Low Energy Antiprotons, Villars sur Ollon, 1987, (Harwood Academic, Chur, 1988), p. 19.

[12] A. Wolf, L. Hütten and H. Poth, Magnetic field measurements in the electron cooling device for LEAR, KfK 3718 (1984).

[13] C. Habfast, H. Poth, B. Seligmann, A. Wolf, J. Berger, P. Blatt, P. Hauck, W. Meyer and R. Neumann, Appl. Phys. B44 (1987) 87.

[14] M. Bell and J.S. Bell, Part. Accel. 12 (1982) 49.

[15] E.N. Dementiev, N.S. Dikansky, A.S. Medvedko, V.V. Parkhomchuk and D.V. Pestrikov, Sov. Phys. Tech. Phys. 25 (1980) 1001.

[16] V.V. Parkhomchuk and D.V. Pestrikov, Sov. Phys. Tech. Phys. 25 (1980) 818.

[17] A. Hofmann, Single-beam collective phenomena-longitudinal in CERN 77-13 (1977), p. 139.

[18] S. Chattopadhyay, Some fundamental aspects of fluctuations and coherence in charged-particle beams in storage rings, CERN 84-11 (1984).

[19] M. Abramowitz and I.A. Stegun, Handbook of mathematical functions (Dover, New York, 1965), Chapter 7.

Table 1

Electron cooler data for this experiment

Acceleration voltage, U	27.660	11.786	kV
Typical beam energy on axis, E_0	26.929	11.480	keV
Corresponding velocity, β_0	0.31	0.21	c
Gun perveance	0.55	0.55	10^{-6} $A \cdot V^{-3/2}$
Typical beam current	2.6, 1.3, 0.6	0.7	A
Beam radius, a	2.5	2.5	cm
Electron density, n_e	8.3×10^7	3.5×10^7	cm^{-3}
Magnetic field strength B_0	455	303	G
Length of interaction region, ℓ	1.5	1.5	m
Typical vacuum in interaction region	7×10^{-11}	3×10^{-11}	Torr

Table 2

LEAR parameters relevant to electron cooling

Nominal proton-beam energy	49.446	21.0	MeV
Beam rigidity (= 3.3 $\beta\gamma$), Bρ	0.99	0.66	T·m
Corresponding velocity, β	0.31	0.21	c
Number of stored protons, N_p	10^7 to 3×10^9	7×10^7	
Initial beam emittance (95%), ε	30	30	π mm·mrad
Initial momentum spread, $\Delta p/p$	3×10^{-3}	3×10^{-3}	
Ring circumference, C	78.592	78.592	m
Nominal revolution frequency, f_0	1.192	0.795	MHz
Length of neutral channel, L	9.3	9.3	m
Horizontal β in cooling section, β_h	1.9	1.9	m
Vertical β in cooling section, β_v	5.3	5.3	m
Momentum dispersion in cooling region, D	3.6	3.6	m
Transition energy, γ_t	4.7i	4.7i	
$\eta = 1 - \beta^2 + 1/\gamma_t^2$	0.95	1.00	
Horizontal betatron tune, Q_h	2.305		
Vertical betatron tune, Q_v	2.730		

Figure captions

Fig. 1: Layout of LEAR; the inset shows the electron cooler in more detail.

Fig. 2: Signal from an electrostatic pick-up after a kick showing the coupling of emittances due to the cooler solenoid field.

Fig. 3: Illustration of the radial velocity profile within the electron beam and the distribution of the protons along the dispersion line. The cooling force drags the protons to the lower crossing point between the parabola and the dispersion line.

Fig. 4: a) Frequency spectrum of a proton beam just after injection without cooling. Second trace: after a few seconds of electron cooling.
b) Frequency spectra taken every second after injection.

Fig. 5: Hydrogen-beam profile measured at 9.3 m downstream of the cooling section (cooled beam).

Fig. 6: Time evolution of the Schottky-signal intensity after an acceleration voltage step of 200 V: a) in a certain frequency span between the initial and the final value, b) with the frequency band at the final position.

Fig. 7: Frictional force as a function of the proton velocity in the electron rest frame. In order to obtain the values in the laboratory frame one has to multiply by ℓ/C.

Fig. 8: Frequency spectrum of a proton beam after stochastic heating (rectangular trace) and after cooling to equilibrium.

Fig. 9: Time evolution of the Schottky-noise power in a small frequency bandwidth centred around the frequency shown in Fig. 8 (for the position after cooling).

Fig. 10: Total cooling time as a function of the initial proton momentum spread.

Fig. 11: a) Equilibrium momentum spread with simultaneous stochastic heating of the proton beam (25 μW/Hz, 32 kHz).
b) Equilibrium momentum width and transverse temperature as a function of the total stochastic heating power.

Fig. 12: Equilibrium momentum spread as a function of the modulation amplitude of the acceleration voltage for the electrons.

Fig. 13: Recombination rate as a function of the modulation amplitude.

Fig. 14: Revolution frequency of the proton beam as a function of the electron acceleration voltage for different electron-beam currents. The arrows indicate the acceleration voltage U_0 for which the electron-beam energy on the axis matches the nominal proton revolution frequency f_0.

Fig. 15: Frequency spectrum of the transverse Schottky pick-up electrode: a) uncooled beam, b) partially cooled stable beam, c) cooled unstable beam.

Fig. 16: Evolution of horizontal and vertical beam emittances as a function of time after cooling was activated. These values are obtained from horizontal (□) and vertical (◆) Schottky signals. The power on a large bandwidth containing a satellite is recorded as a function of time. The noise is quadratically subtracted from the signal.

Fig. 17: Longitudinal noise signal of cold proton beam: a) measured signal for 10^9 protons, b) calculated signal for 2×10^9 stored protons and r.m.s. momentum spreads from 1.4 to 3.9×10^{-5} (lowest dip), c) distance d of the maxima in units of f_c, as a function of $s = \Delta f/f_c$, d) relative depth of the dip, 1-T, as a function of s. (See Appendix).

Fig. 18: Momentum spread deduced from the collective noise signal as a function of beam intensity. Results of other experiments as discussed in the text.

Fig. 19: The evolution of the 10th harmonic of the bunch signal, observed on one of the LEAR position pick-ups (sum signal) after cooling is activated (logarithmic scale of 5 dB/div.).

Fig. 20: Time distribution of the hydrogen atoms with respect to the RF phase for a bunched proton beam (U_{RF} = 100 V).

Fig. 21: Bunch length as a function of RF voltage.

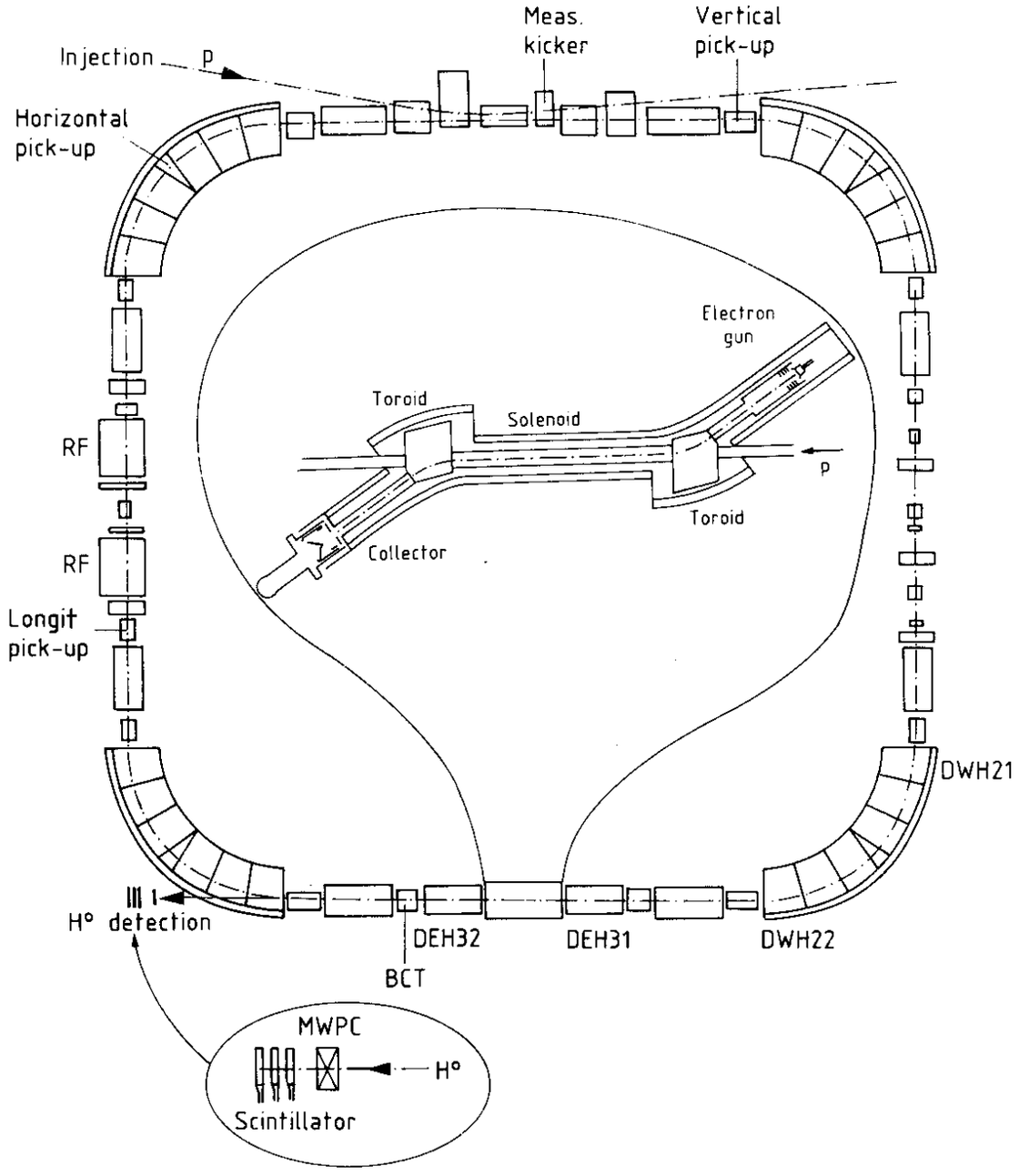
Meas.
kicker
Vertical
pick-up
Injection
p
Horizontal
pick-up
Electron
gun
Toroid
Solenoid
RF
p
RF
Toroid
Collector
Longit
pick-up
DWH21
H° detection
DEH32
DEH31
DWH22
BCT
MWPC
H°
Scintillator

Fig. 1

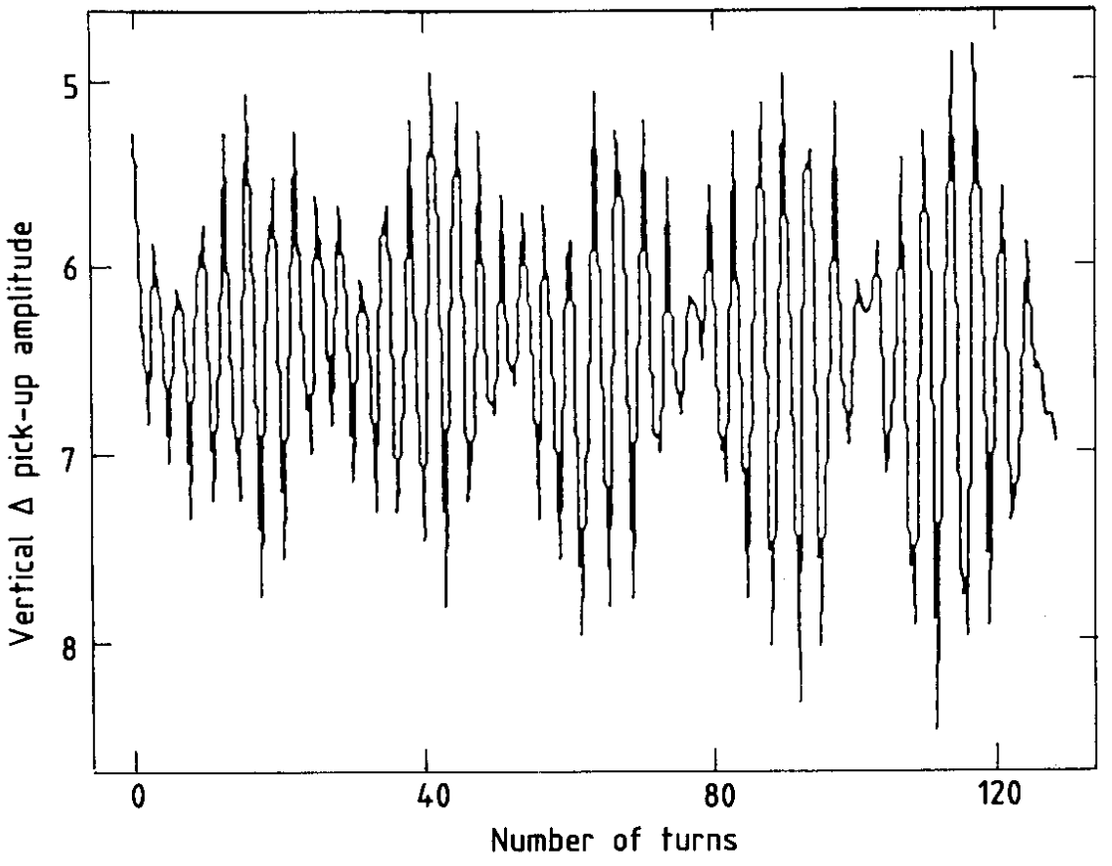
Vertical Δ pick-up amplitude
5
6
7
8
0
40
80
120
Number of turns

Fig. 2

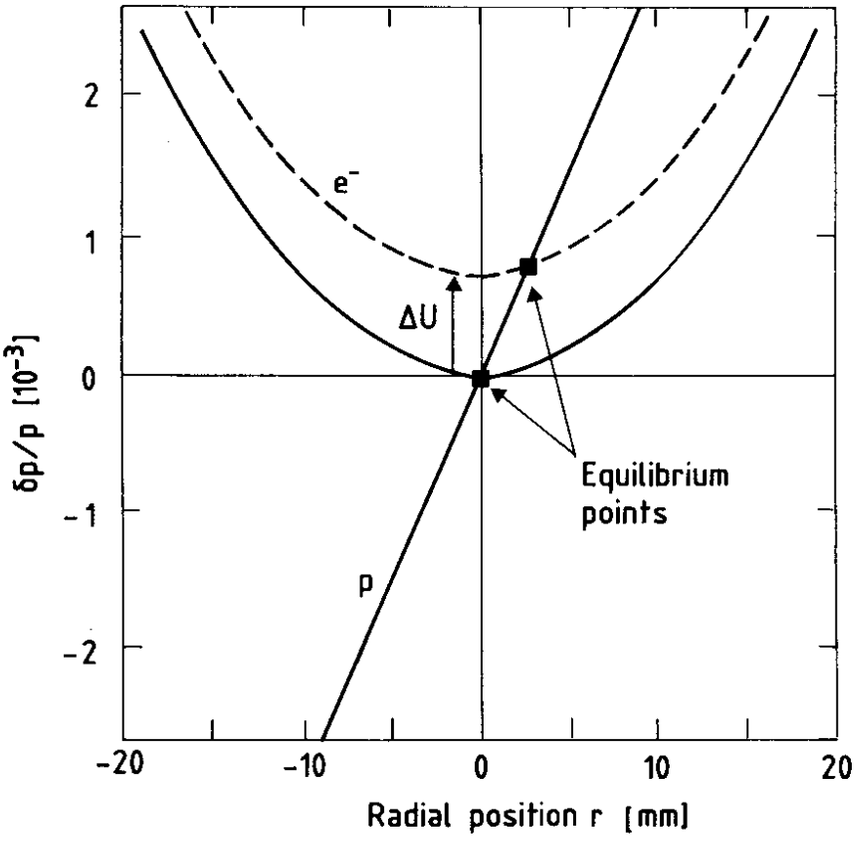
δp/p [10⁻³]
2
1
0
-1
-2
e⁻
ΔU
p
Equilibrium points
-20
-10
0
10
20
Radial position r [mm]

Fig. 3

a)

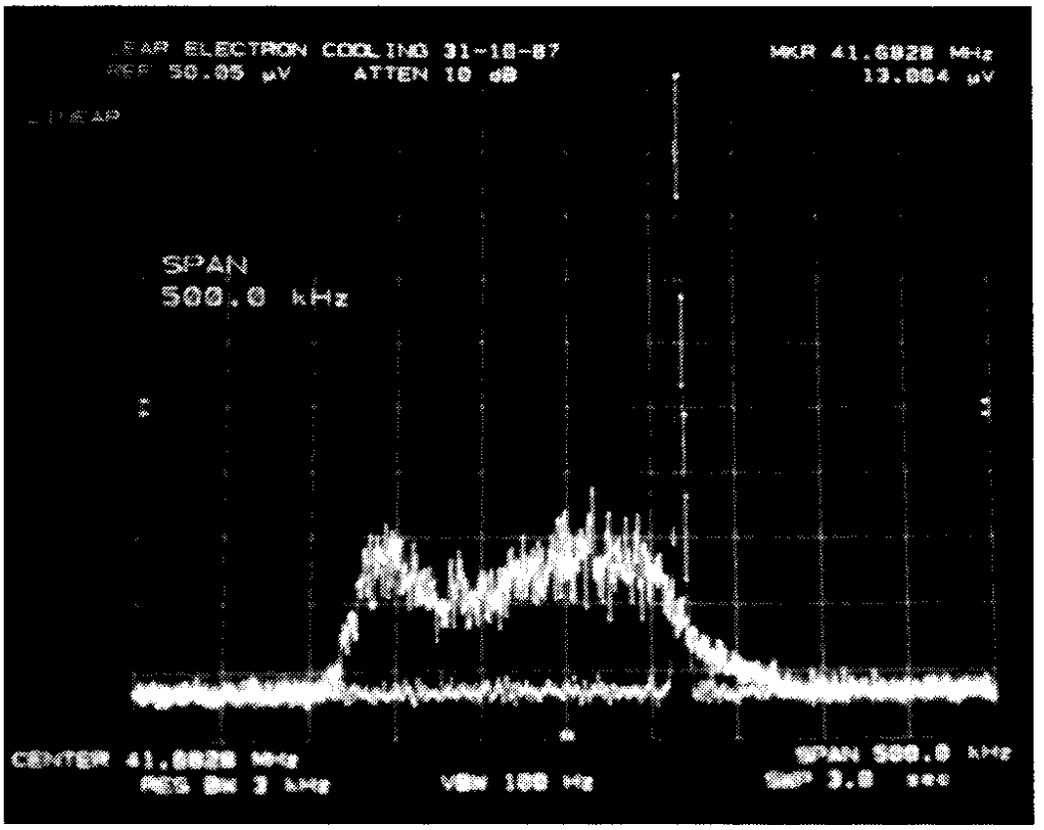
ELECTRON COOLING 31-10-87
ATTEN 10 dB
SPAN
500.0 kHz

b)

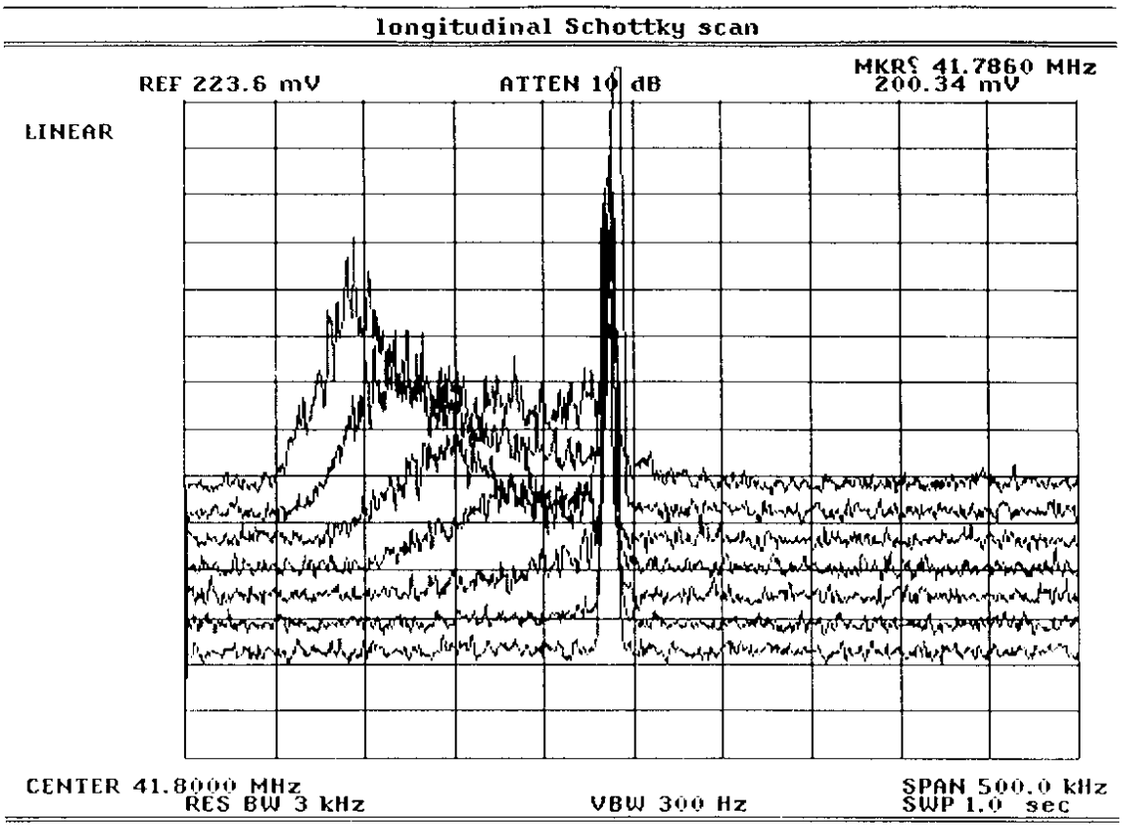
longitudinal Schottky scan
REF 223.6 mV
ATTEN 10 dB
MKR 41.7860 MHz
200.34 mV
LINEAR
CENTER 41.8000 MHz
RES BW 3 kHz
VBW 300 Hz
SPAN 500.0 kHz
SWP 1.0 sec

Fig. 4

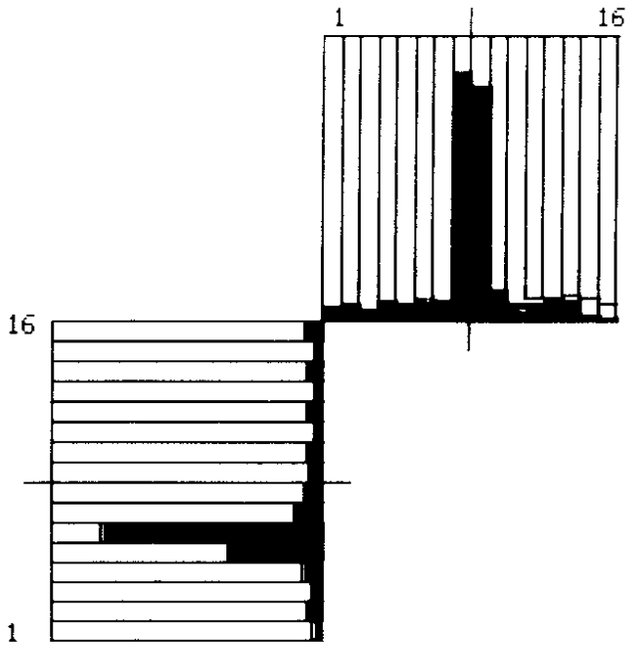
1
16
16
1

Fig. 5

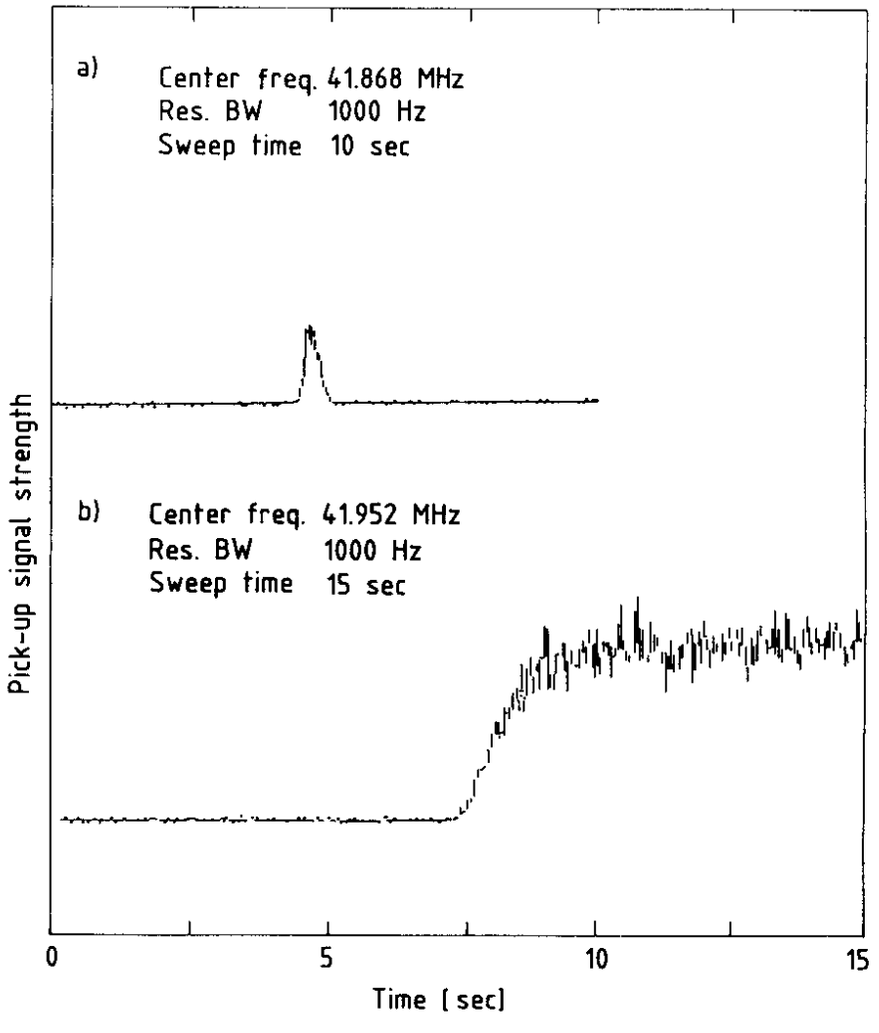
a)
Center freq. 41.868 MHz
Res. BW 1000 Hz
Sweep time 10 sec
b)
Center freq. 41.952 MHz
Res. BW 1000 Hz
Sweep time 15 sec
Pick-up signal strength
0
5
10
15
Time [sec]

Fig. 6

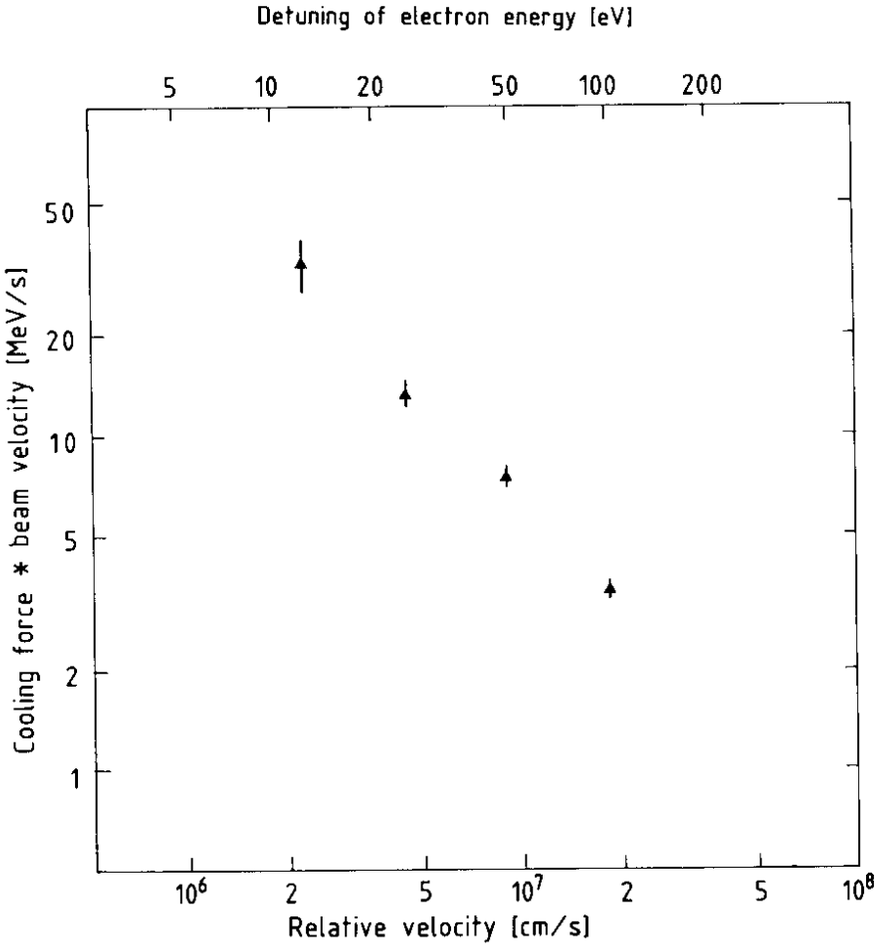
Detuning of electron energy [eV]
5
10
20
50
100
200
50
20
10
5
2
1
Cooling force * beam velocity [MeV/s]
10^6
2
5
10^7
2
5
10^8
Relative velocity [cm/s]

Fig. 7

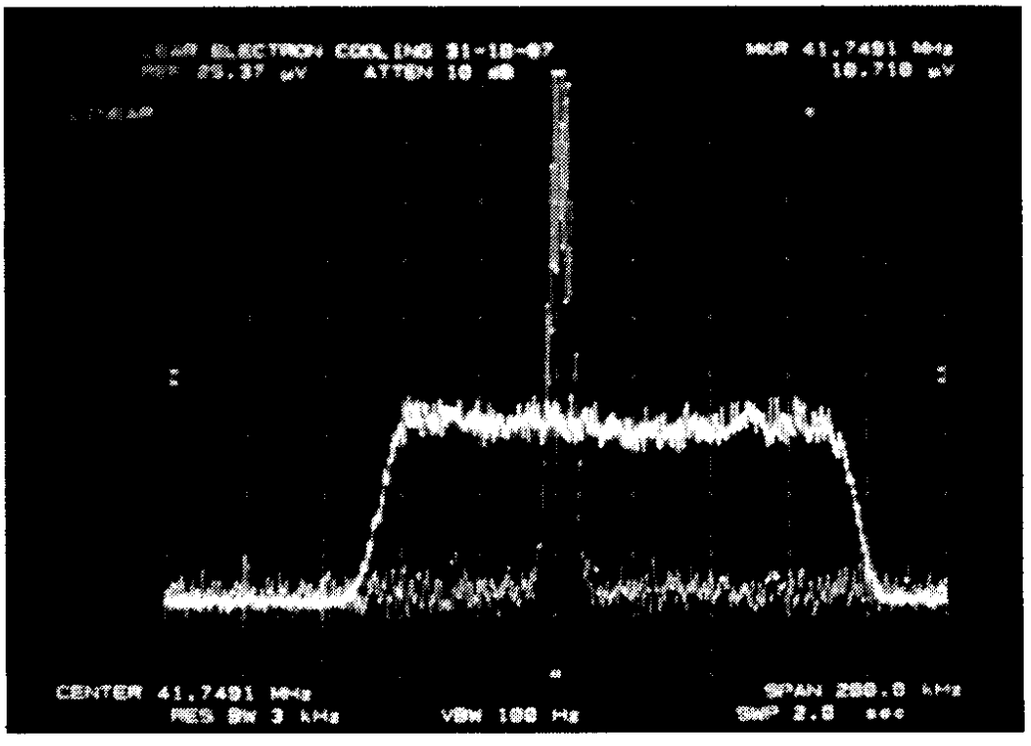
CENTER 41.7491 MHz
RES BW 3 kHz
VBW 100 Hz
SPAN 200.0 kHz
SWP 2.0 sec

Fig. 8

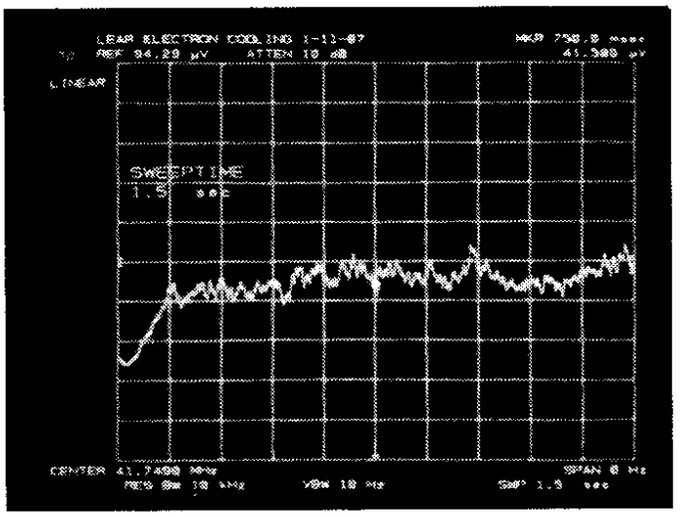
LINEAR
SWEEPTIME

Fig. 9

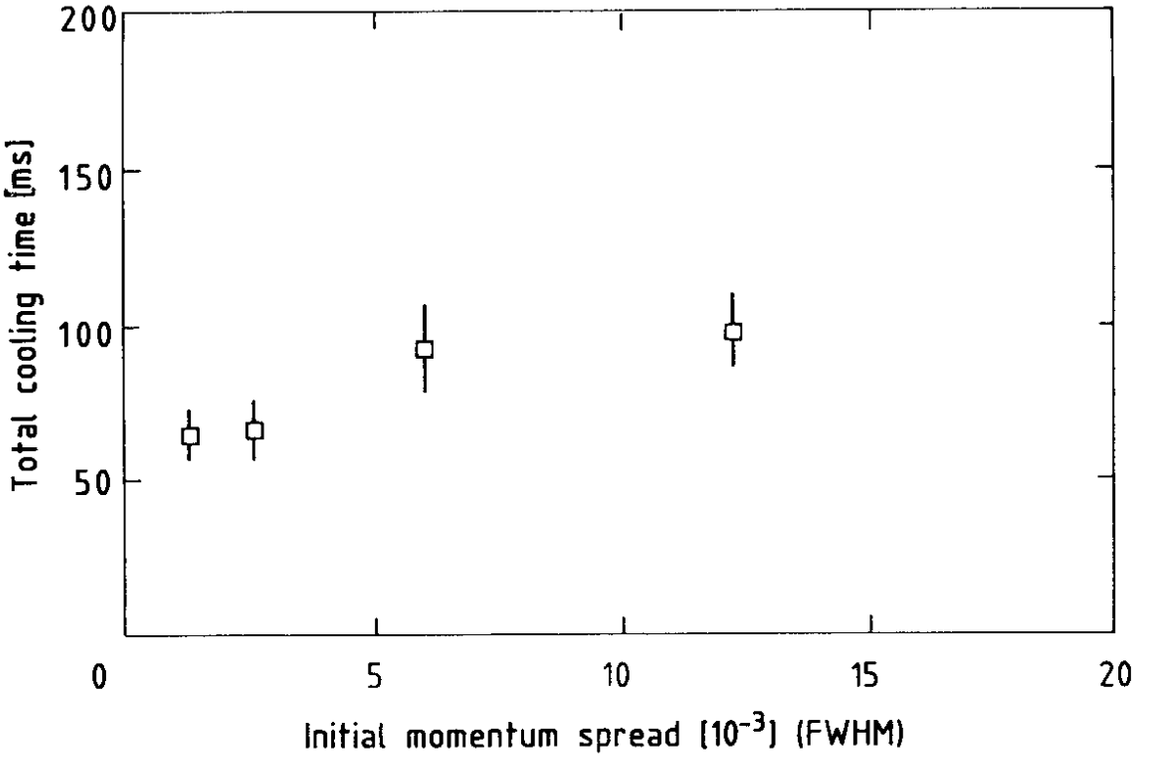
200
150
100
50
0
5
10
15
20
Total cooling time [ms]
Initial momentum spread [10^{-3}] (FWHM)

Fig. 10

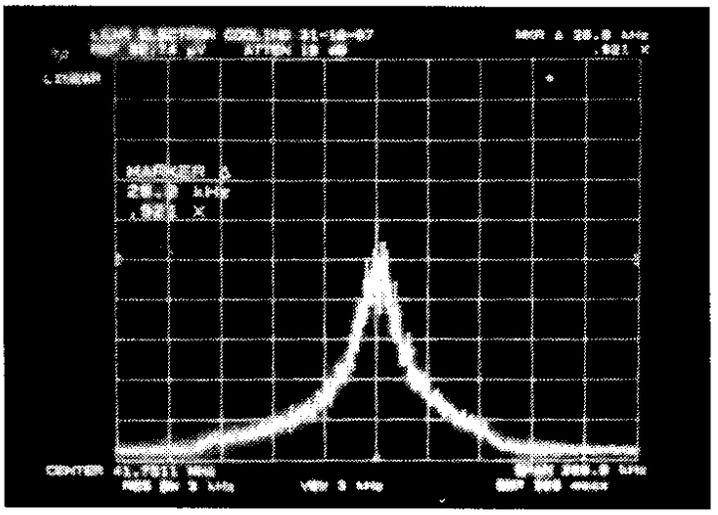

a)

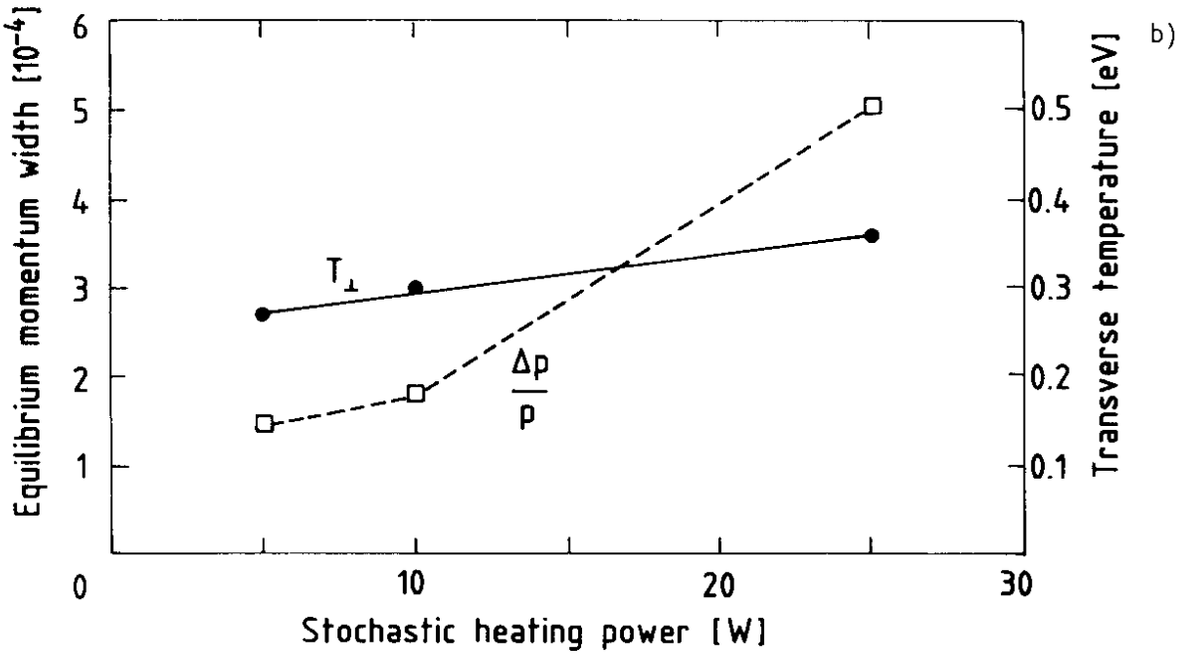
Equilibrium momentum width [10⁻⁴]
Transverse temperature [eV]
Stochastic heating power [W]
T⊥
Δp/p
0
1
2
3
4
5
6
0.1
0.2
0.3
0.4
0.5
10
20
30

b)

Fig. 11

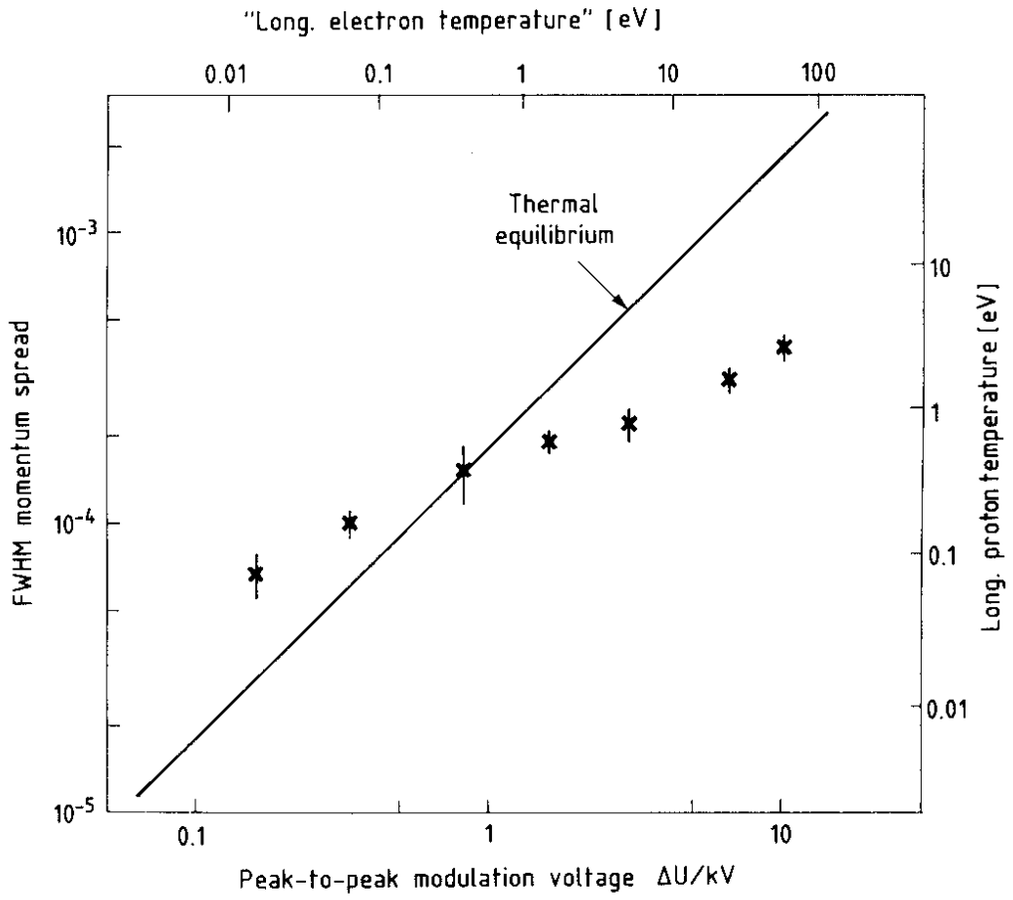
"Long. electron temperature" [eV]
0.01
0.1
1
10
100
Thermal
equilibrium
10^{-3}
10^{-4}
10^{-5}
FWHM momentum spread
10
1
0.1
0.01
Long. proton temperature [eV]
0.1
1
10
Peak-to-peak modulation voltage ΔU/kV

Fig. 12

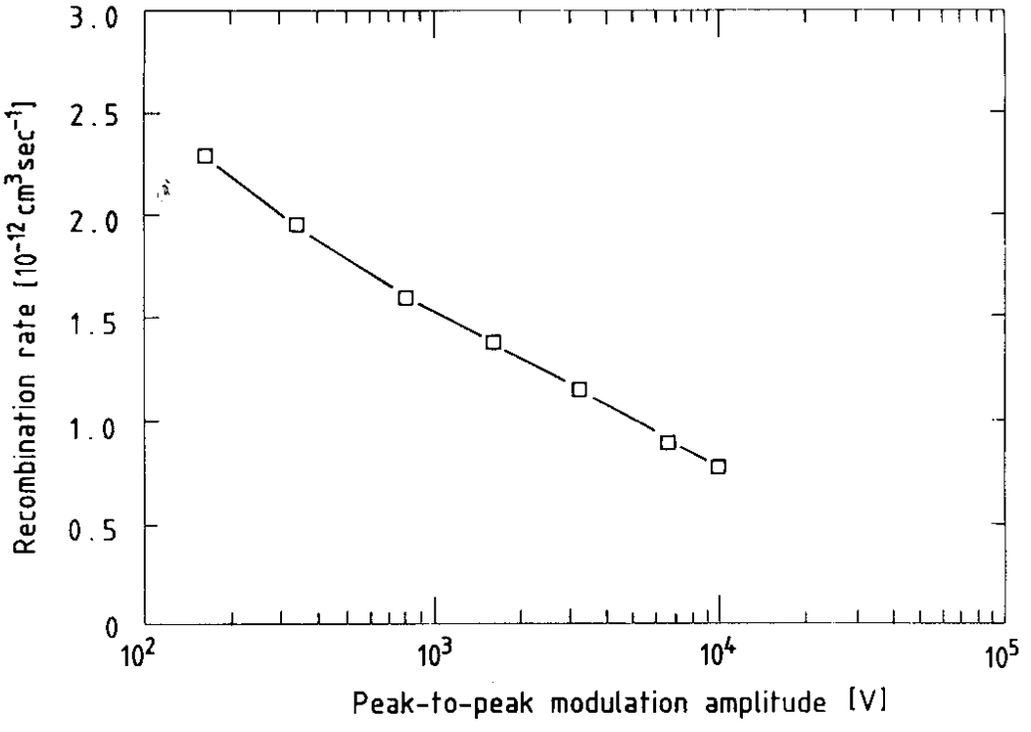
3.0
2.5
2.0
1.5
1.0
0.5
0
Recombination rate [10^{-12} cm^{3}sec^{-1}]
10^2
10^3
10^4
10^5
Peak-to-peak modulation amplitude [V]

Fig. 13

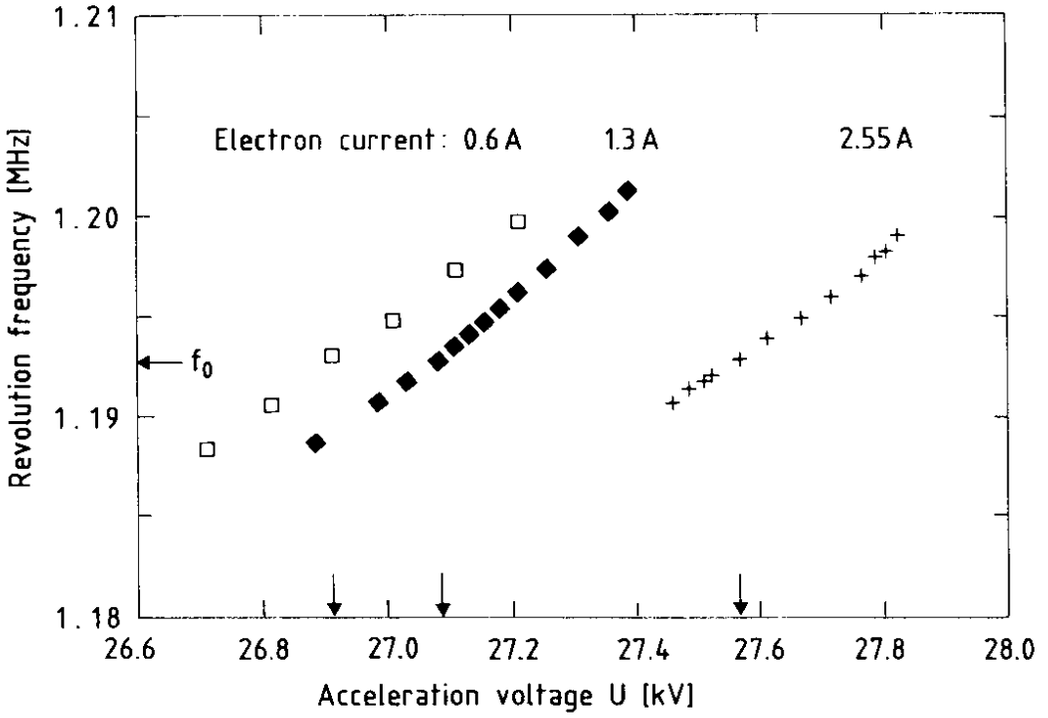
1.21
1.20
1.19
1.18
Revolution frequency [MHz]
Electron current: 0.6 A
1.3 A
2.55 A
f_0
26.6
26.8
27.0
27.2
27.4
27.6
27.8
28.0
Acceleration voltage U [kV]

Fig. 14

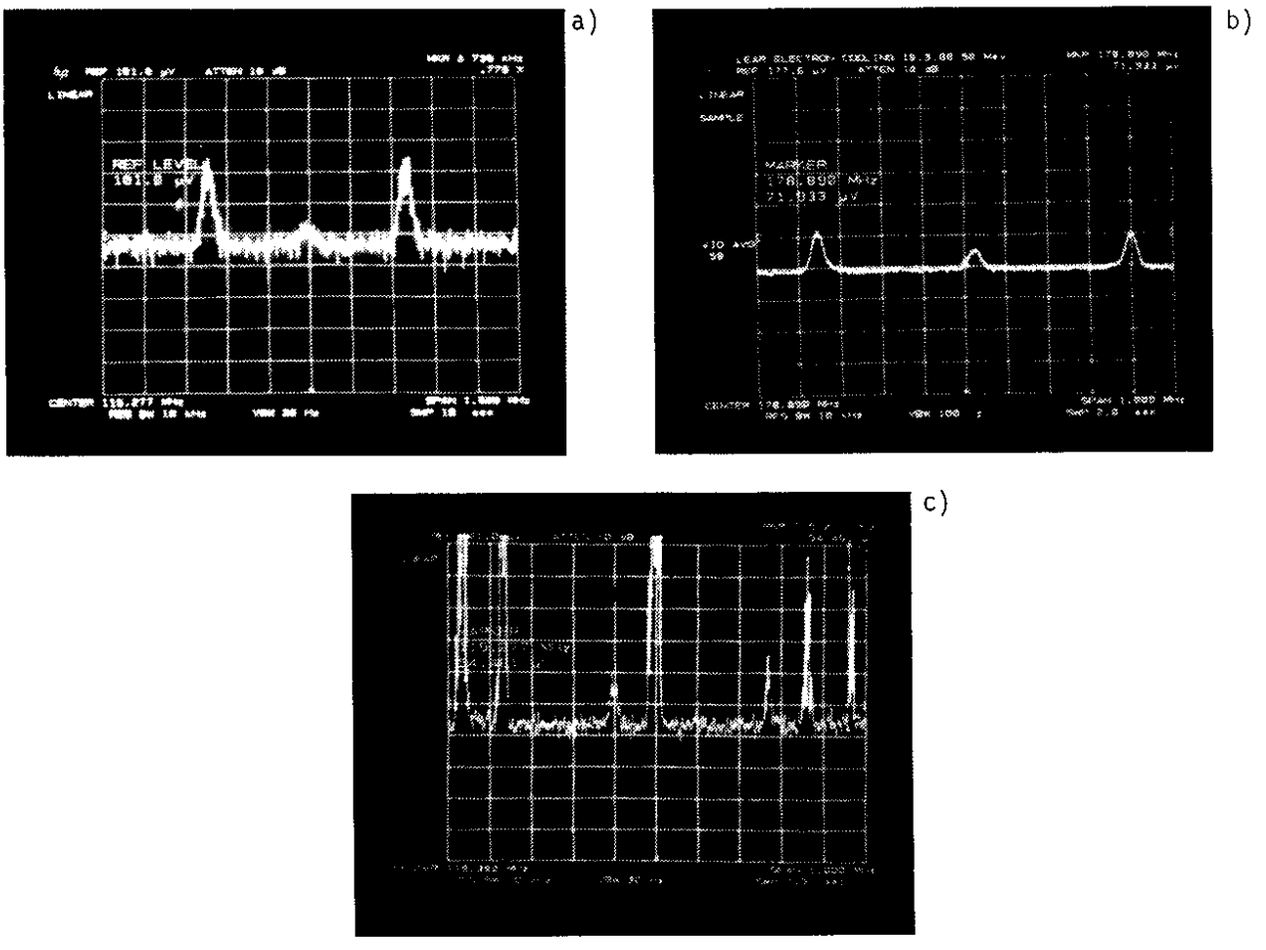
a)
b)
c)

Fig. 15

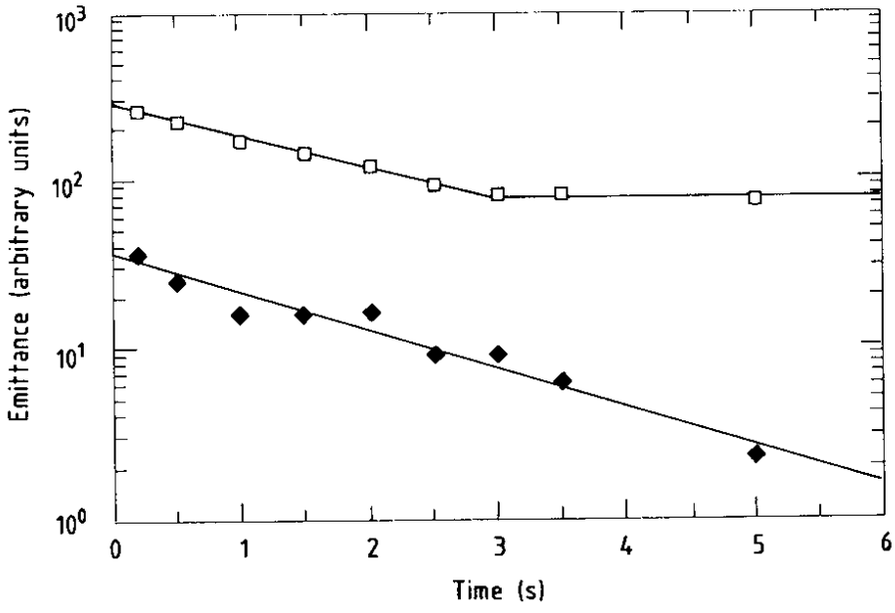
Emittance (arbitrary units)
10^3
10^2
10^1
10^0
0
1
2
3
4
5
6
Time (s)

Fig. 16

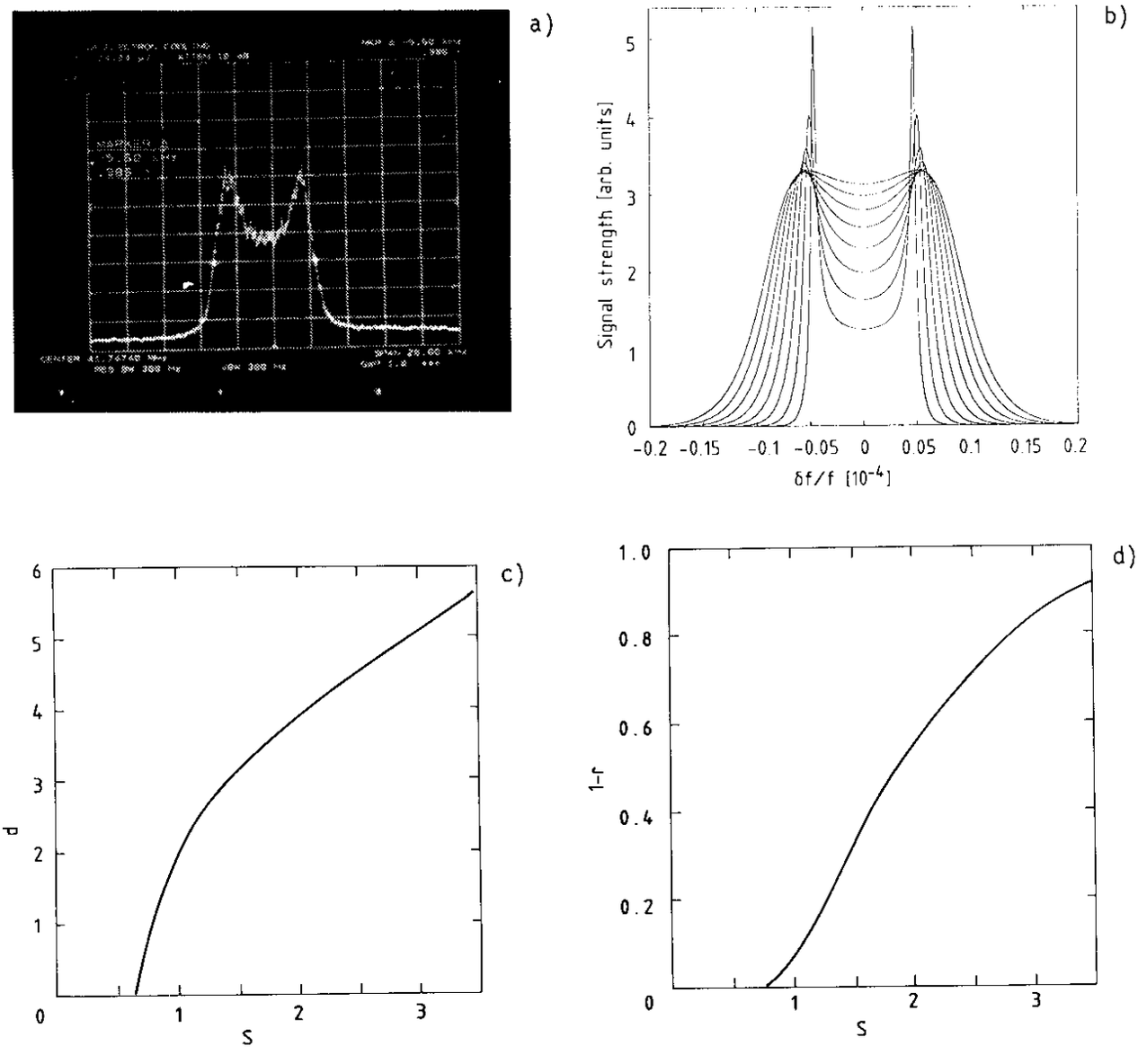
a)
b)
Signal strength [arb. units]
δf/f [10^{-4}]
c)
d
S
d)
1-r
S

Fig. 17

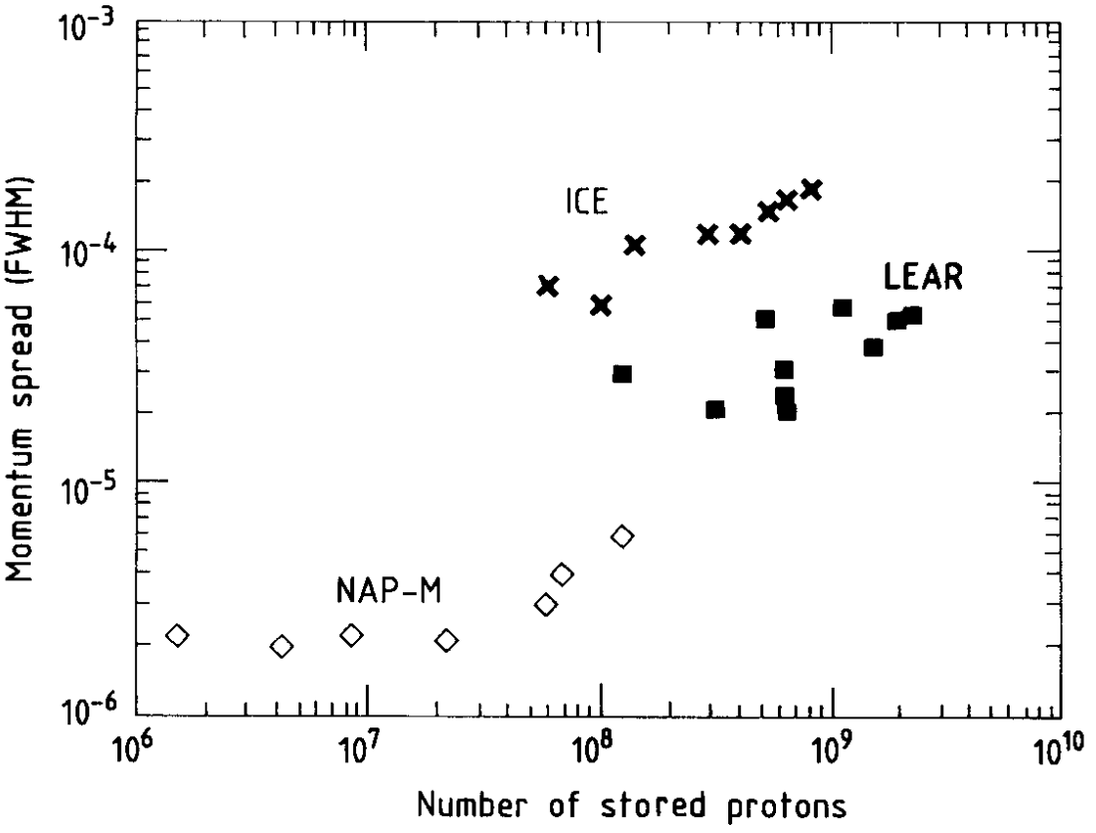
Momentum spread (FWHM)
10^{-3}
10^{-4}
10^{-5}
10^{-6}
ICE
LEAR
NAP-M
10^{6}
10^{7}
10^{8}
10^{9}
10^{10}
Number of stored protons

Fig. 18

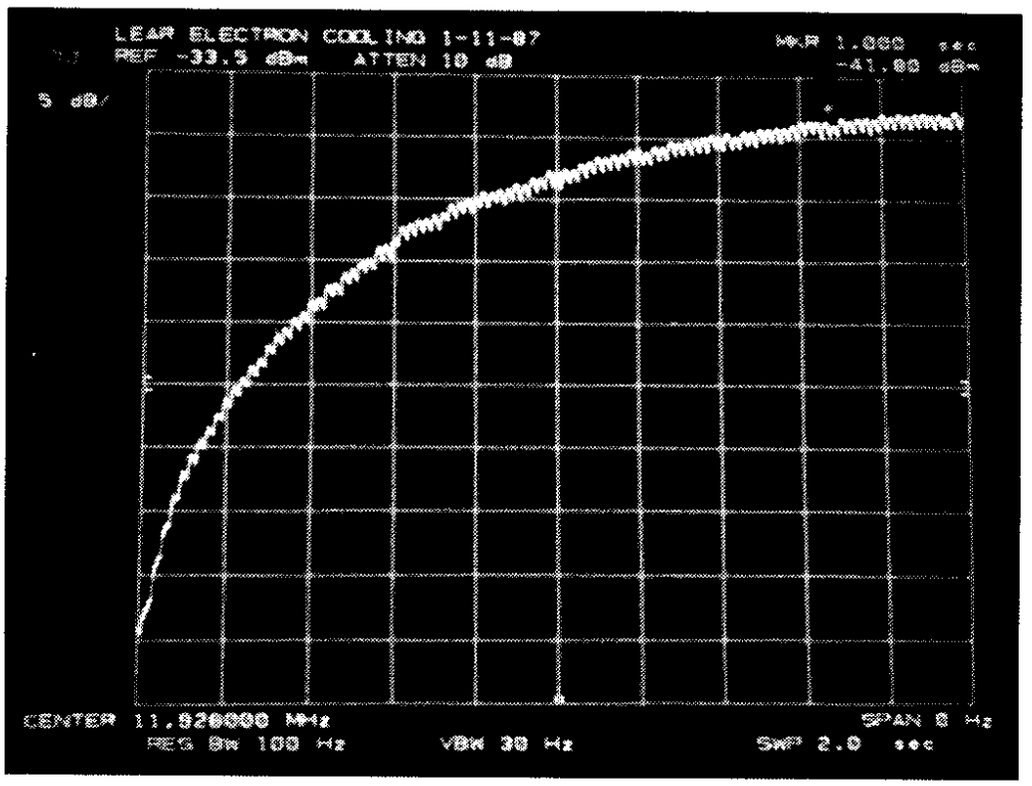
LEAR ELECTRON COOLING 1-11-87
REF -33.5 dBm
ATTEN 10 dB
5 dB/
CENTER 11.926000 MHz
RES BW 100 Hz
VBW 30 Hz
SPAN 0 Hz
SWP 2.0 sec

Fig. 19

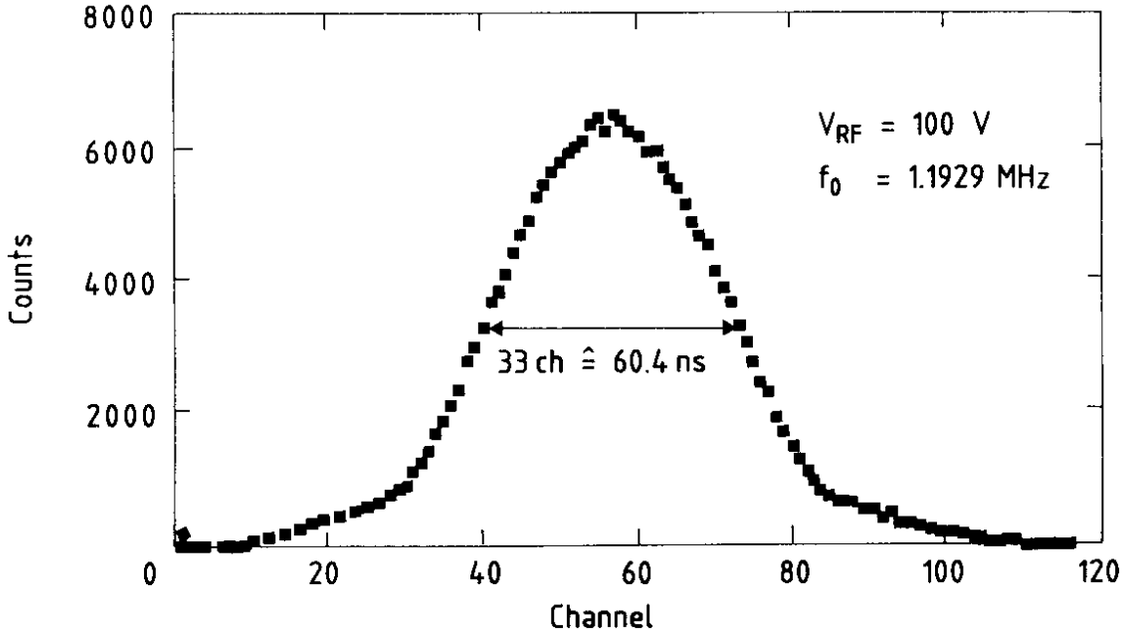
8000
6000
4000
2000
0
Counts
20
40
60
80
100
120
Channel
V_{RF} = 100 V
f_0 = 1.1929 MHz
33 ch ≙ 60.4 ns

Fig. 20

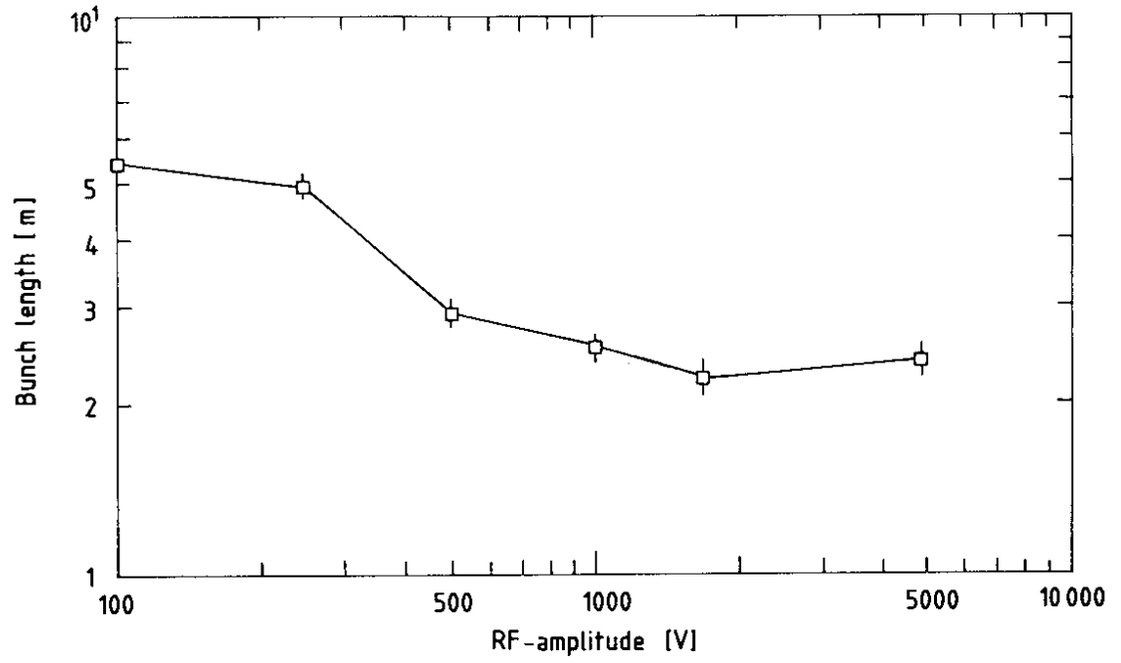
10^1
5
4
3
2
1
Bunch length [m]
100
500
1000
5000
10 000
RF-amplitude [V]

Fig. 21